Evidence for a diachronous Late Permian marine crisis from the Canadian Arctic region

Thomas Algeo[1,†], Charles M. Henderson[2], Brooks Ellwood[3], Harry Rowe[4], Erika Elswick[5], Steven Bates[6], Timothy Lyons[6], James C. Hower[7], Christina Smith[1], Barry Maynard[1], Lindsay E. Hays[8], Roger E. Summons[8], James Fulton[9], and Katherine H. Freeman[10]

[1]*Department of Geology, University of Cincinnati, Cincinnati, Ohio 45221-0013, USA*
[2]*Department of Geoscience, University of Calgary, Calgary, Alberta T2N 1N4, Canada*
[3]*Department of Geology and Geophysics, Louisiana State University, Baton Rouge, Louisiana 70803, USA*
[4]*Department of Earth and Environmental Sciences, University of Texas at Arlington, Arlington, Texas 76019, USA*
[5]*Department of Geological Sciences, Indiana University, Bloomington, Indiana 47405, USA*
[6]*Department of Earth Sciences, University of California, Riverside, California 92521-0423, USA*
[7]*Center for Applied Energy Research and Department of Earth & Environmental Sciences, University of Kentucky, Lexington, Kentucky 40506, USA*
[8]*Department of Earth, Atmospheric, and Planetary Science, Massachusetts Institute of Technology, Cambridge, Massachusetts 02139, USA*
[9]*Woods Hole Oceanographic Institution, 266 Woods Hole Road, Woods Hole, Massachusetts 02543, USA*
[10]*Department of Geosciences, Pennsylvania State University, University Park, Pennsylvania 16802, USA*

ABSTRACT

A high-resolution chemostratigraphic study of a 24-m-thick section at West Blind Fiord on Ellesmere Island (Canadian Arctic) documents stepwise environmental deterioration in the marine Sverdrup Basin during the late Changhsingian (late Late Permian) as a result of volcanic disturbances to surrounding landmasses. A horizon within the upper Lindström Formation (datum A) is characterized by increased Fe-oxyhydroxide fluxes and weathering intensity as well as modest shifts toward more reducing water-mass conditions and higher marine productivity, recording an initial disturbance that washed soils into the marine environment. The contact between chert of the Lindström Formation and silty shale of the overlying Blind Fiord Formation, which is 1.6 m higher and ~50 k.y. younger than datum A, records a large increase in detrital sediment flux, more strongly enhanced marine productivity, and a regional extinction of siliceous sponges, herein termed the "Arctic extinction event." The horizon equivalent to the latest Permian mass extinction of Tethyan shallow-marine sections is 5.6 m higher and ~100 k.y. younger than the Arctic extinction event, demonstrating the diachronous nature of the marine biotic and environmental crisis at a global scale; it is associated with intensified anoxia and possible changes in phytoplankton community composition in the study section. Marine environmental deterioration in the Sverdrup Basin, probably triggered by terrestrial ecosystem deterioration and elevated detrital sediment fluxes, was under way by the early part of the late Changhsingian, well before the onset of main-stage Siberian Traps flood basalt volcanism. The event sequence at West Blind Fiord may record the deleterious effects of early-stage explosive silicic eruptions that affected the Boreal region, possibly through deposition of toxic gas and ash within a restricted latitudinal band, while having little impact on marine ecosystems in the peri-equatorial Tethyan region.

INTRODUCTION

The latest Permian mass extinction was the largest mass extinction in Earth history, during which ~90% of marine and a large fraction of terrestrial taxa died out (Erwin, 1994; Retallack, 1995; Alroy et al., 2008). In shallow-marine carbonate facies from South China and elsewhere across the Tethyan region, the latest Permian mass extinction was generally an abrupt event of latest Changhsingian age, associated with rapid onset of water-column anoxia and correlative with a negative shift of 3‰–4‰ in carbonate $\delta^{13}C$ (Rampino and Adler, 1998; Jin et al., 2000; Algeo et al., 2007; Lehrmann et al., 2007; Chen et al., 2010). Contemporaneously, the largest eruption of flood basalts during the Phanerozoic produced the Siberian Traps, the age of which is indistinguishable from that of the ca. 252 Ma Permian-Triassic boundary (Campbell et al., 1992; Reichow et al., 2009; Mundil et al., 2010). Based on such observations, it has been widely inferred that the latest Permian mass extinction was a globally synchronous event triggered by the (main-stage) eruptions of the Siberian Traps volcanic province (e.g., Benton and Twitchett, 2003; Korte et al., 2010).

Recent studies of intermediate-depth marine facies from South China have yielded a somewhat different view regarding the pattern of extinction associated with the latest Permian mass extinction. One of the best studied sections is at Dongpan, in southern Guangxi Province, where radiolarian chert and siliceous mudstone accumulated at water depths of 200–500 m (He et al., 2005, 2007; Yin et al., 2007). There, the main extinction episode occurred in a stepwise manner over an ~2-m-thick interval: Radiolarians were decimated at the base of Bed 6, ostracods at the base of Bed 10, and brachiopods and foraminifera at the base of Bed 11 (He et al., 2005, 2007; Feng et al., 2007; Shen et al., 2012). A prominent bentonite in the middle of this interval (Bed 9) has been correlated with the ash layer representing the latest Permian mass extinction (Bed 25)

†E-mail: thomas.algeo@uc.edu

GSA Bulletin; September/October 2012; v. 124; no. 9/10; p. 1424–1448; doi: 10.1130/B30505.1; 16 figures; Data Repository item 2012072.

at Meishan D, the global stratotype section and point (GSSP) for the Permian-Triassic boundary (Yin et al., 2001). A similar pattern of stepwise extinction was reported from the Chaotian section in northern Sichuan Province, where the main radiolarian crisis is located 3.5 m below the latest Permian mass extinction (Isozaki et al., 2007a). At both Dongpan and Chaotian, the extinction sequence was probably the result of depth-related environmental changes. As the oxygen-minimum zone intensified and expanded, taxa occupying progressively shallower habitats were adversely affected (Shen et al., 2012). These studies are significant in showing that (1) major biotic and environmental changes were under way at intermediate water depths in the Tethyan region prior to the latest Permian mass extinction defined by shallow-marine facies, and (2) pre–latest Permian mass extinctions among deeper-dwelling organisms such as radiolarians are a manifestation of a globally diachronous extinction event with a minimum duration of about 100 k.y.

Although less well documented, major environmental and biotic changes were under way prior to the latest Permian mass extinction in intermediate-depth marine settings on the northern Pangean margin as well. The marine biota in the Sverdrup Basin of the Canadian Arctic was in decline from the early part of the Late Permian, culminating in a major extinction of sponges in the early part of the late Changhsingian (Henderson and Baud, 1997; Beauchamp and Baud, 2002; Gates et al., 2004; Beauchamp et al., 2009), which we herein designate the "Arctic extinction event." The uppermost 50 m section of the Black Stripe Formation at Buchanan Lake is characterized by a gradual ~3‰ negative shift in $\delta^{13}C_{org}$ that was punctuated by three episodes of fly ash loading inferred to represent deposition of airborne combustion products of magmatic intrusions into Siberian coalfields (Grasby et al., 2011). This negative $\delta^{13}C_{org}$ shift commenced during the early late Changhsingian *Clarkina bachmanni* zone (Korte and Kozur, 2010), and it predates the ~3‰–4‰ negative shift in marine carbonate $\delta^{13}C$ records globally (Luo et al., 2011). Based on average sedimentation rates, Grasby et al. (2011) estimated that the onset of the $\delta^{13}C_{org}$ shift at Buchanan Lake preceded the latest Permian mass extinction by ~500–750 m.y.; however, Shen et al. (2010) correlated the *C. bachmanni* zone to the lower *C. yini* zone and estimated its age as only ~200–300 k.y. older than the latest Permian mass extinction. Collectively, these studies show that major changes in marine biotas and environmental conditions were under way in the Boreal region from the early part of the late Changhsingian, well in advance of the latest Permian mass extinction, and that such changes may have been caused by early (pre–main-stage) eruptions of the Siberian Traps volcanic province (cf. Kozur and Weems, 2011).

The goals of the present study are to better understand (1) environmental changes in intermediate-depth marine facies of the Sverdrup Basin prior to the latest Permian mass extinction, (2) the timing of these changes in relation to marine extinction events in the Canadian Arctic and elsewhere globally, and (3) the causes of environmental stress and regional biotic decline prior to the latest Permian mass extinction. For this purpose, we undertook a multiproxy chemostratigraphic analysis of a 24-m-thick interval of the uppermost Permian at West Blind Fiord on southwestern Ellesmere Island. We generated chemostratigraphic profiles at a high level of stratigraphic resolution, with 56 samples from an interval representing ~500 k.y., or an average of one sample per ~10 k.y. These data were used to assess the hypothesis that environmental changes were under way in intermediate-depth marine settings at mid-northern paleolatitudes (~40°N) at least 100 k.y. prior to the latest Permian mass extinction, as defined by extinction patterns in peri-equatorial (Tethyan) shallow-marine facies.

GEOLOGIC SETTING—SVERDRUP BASIN

Paleogeography and Climate

The Sverdrup Basin is a >1000-km-long, 400-km-wide, northeast-trending pericratonic successor basin underlying the northernmost islands of the Canadian Arctic region (Embry, 1991; Embry and Beauchamp, 2008; Fig. 1A). The basin developed through rifting and collapse of the Franklinian geosyncline following the Late Devonian–Mississippian Ellesmerian orogeny (Beauchamp et al., 1989a). During the Permian–Triassic, it was surrounded by landmasses to the north, east, and south but linked to the global ocean via a shallow strait on its western margin (Reid et al., 2007; Embry, 2009). This strait existed throughout the late Paleozoic except for transient episodes of closure in the early Pennsylvanian and, possibly, in the Late Permian (Beauchamp et al., 1989b). The basin achieved its present configuration when the northern landmass (termed "Crockerland" by Beauchamp et al., 1989a; Embry, 2009) rifted away during Early Cretaceous opening of the Canada Basin of the Arctic Ocean (Plafker and Berg, 1994; Symons and McCausland, 2006).

Climatic conditions in the Sverdrup Basin region evolved from warm and dry in the Early Permian to cool and humid in the Late Permian (Beauchamp, 1994; Beauchamp and Baud, 2002; Reid et al., 2007). Around the margin of the basin, sedimentary facies included glauconitic sandstone, siltstone, and red shale of marginal marine to nonmarine character containing a low-diversity, temperate-zone fossil assemblage dominated by sponges, bryozoans, echinoderms, and brachiopods. Concurrently, the basin center accumulated a >5-km-thick succession of dark-gray shale, cherty siltstone, and chert. The high concentration of sponge-derived chert in Upper Permian beds has been interpreted as evidence of vigorous thermohaline circulation and nutrient upwelling in the Panthalassic Ocean, and its absence in Lower Triassic beds has been interpreted as evidence of sluggish circulation and nutrient-poor surface waters (Beauchamp, 1994; Beauchamp and Desrochers, 1997; Beauchamp and Baud, 2002). Water depths in the basin center were probably on the order of a few hundred meters, a depth range favored by modern hexactinellid sponges. The water column was stratified, resulting in enhanced burial of organic carbon in deeper areas and contributing to ^{13}C enrichment of Middle and early Late Permian carbonates in the Sverdrup Basin (Beauchamp et al., 1987) and globally (Isozaki et al., 2007b; Grossman et al., 2008).

Basinal Sequence Stratigraphy

Sedimentation in the center of the Sverdrup Basin was continuous from the Pennsylvanian through the Early Cretaceous, whereas thinner, unconformity-punctuated successions are present on the basin margins (Fig. 1B; Beauchamp et al., 1989b; Beauchamp et al., 2009). The Permian–Triassic is represented by a series of large-scale (third-order, or multimillion-year) transgressive-regressive (T-R) cycles, with Sequence 7 made up of a >200-m-thick upper Capitanian to lower Changhsingian succession, and Sequence 8 represented by an ~350-m-thick middle Changhsingian to Olenekian succession. The study section at West Blind Fiord (section 24 of Beauchamp et al., 2009) was deposited in a slope setting approximately midway between the basin center and southeastern basin margin (Fig. 1B). In this area, the uppermost ~100 m section of the Upper Permian has been assigned to the Black Stripe and Lindström Formations, which are composed of medium-bedded black to white spiculitic cherts passing upward into increasingly argillaceous and thinly bedded siliceous shale, representing the regressive systems tract (RST) of Sequence 7 (Gates et al., 2004; Beauchamp et al., 2009). The sequence boundary between Sequences 7 and 8 is conformable and located ~19 m below the top of the Lindström Formation at West Blind Fiord, although

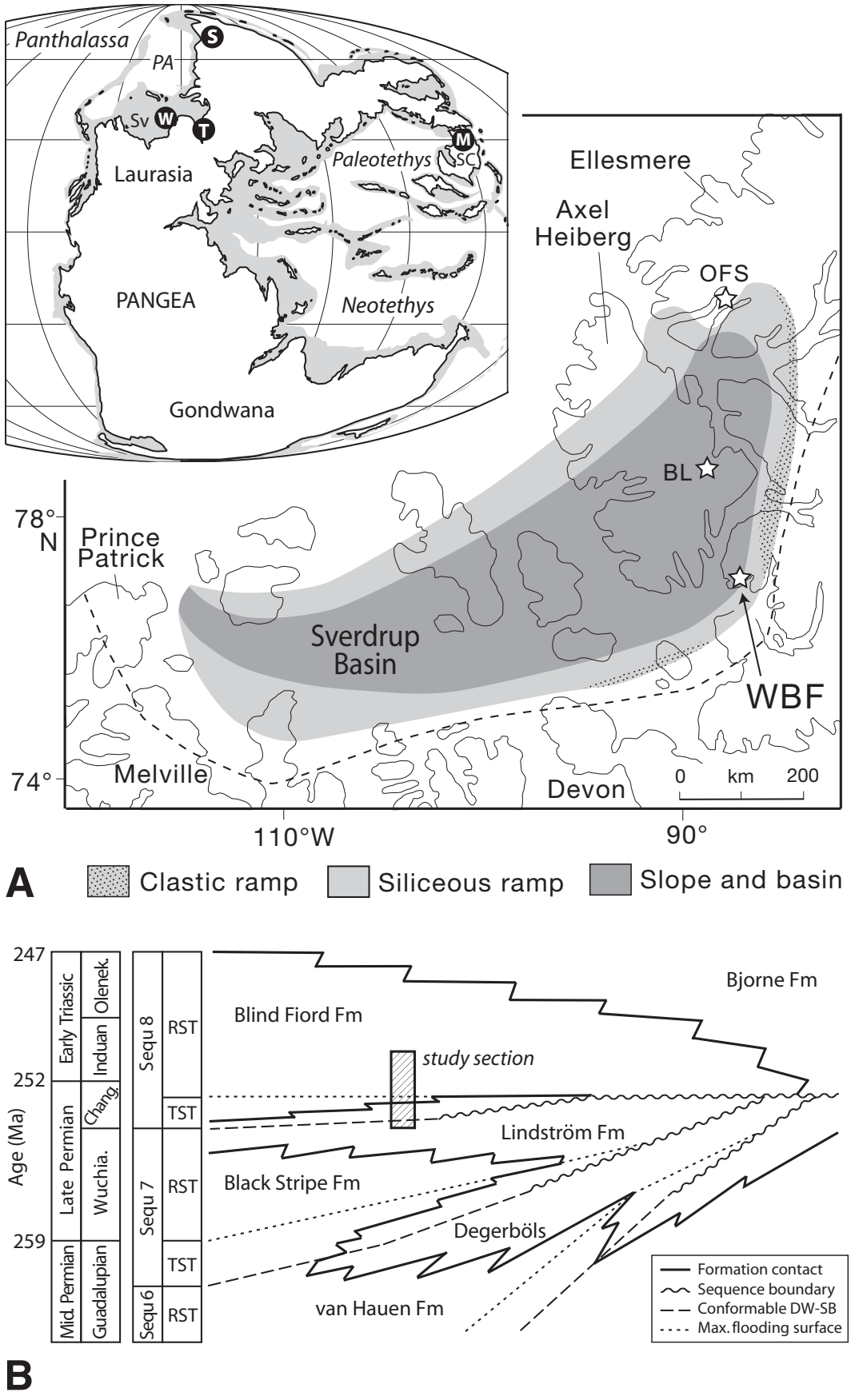

Figure 1. (A) Sverdrup Basin facies map showing the location of the West Blind Fiord (WBF) study section, and the Otto Fiord South (OFS) and Buchanan Lake (BL) sections of Grasby and Beauchamp (2008) and Grasby et al. (2011). The dashed line represents the erosional edge of the basin. The inset map shows global paleogeography at ca. 252 Ma; M—Meishan, PA—paleo-Arctic Ocean, S—Siberian Traps, SC—South China, Sv—Sverdrup Basin, T—Trøndelag, W—West Blind Fiord. (B) Basin-center to basin-margin cross section and sequence stratigraphy of Middle Permian–Lower Triassic units of southern Ellesmere Island. Abbreviations: Wuchia.—Wuchiapingian; Chang.—Changhsingian; Olenek.—Olenekian; Sequ.—sequence; DW-SB—deep-water sequence boundary; RST—regressive systems tract; TST—transgressive systems tract. Note that RST is equivalent to the "highstand systems tract" of some authors, but we retain the sequence terminology of Beauchamp et al. (1989b, 2009) for the Sverdrup Basin succession.

Sequence 8 onlaps progressively older Permian units of Sequence 7 along an unconformity that increases in magnitude and duration more proximally (i.e., closer to the southeastern basin margin). The uppermost part of the Lindström Formation has been interpreted as a transgressive systems tract (TST) capped by a maximum flooding surface at the formation contact with the overlying Blind Fiord Formation (Beauchamp et al., 2009; but see Placement of PTB, LPME, and MFS horizons section). The latter formation consists of finely laminated silty shale overlain by turbiditic siltstone and fine-grained sandstone, representing deposition mainly within the RST of Sequence 8 (Fig. 1B). It has been subdivided into three members, of which only the lowest (the Confederation Point Member; Embry, 1991) is represented in the study section. The study area experienced intermediate burial temperatures (~150–200 °C), as indicated by conodont alteration index (CAI) of 1.5–2.0, thermal alteration index (TAI) of ~3.0, and R_0 of 1.1–2.1 (Utting et al., 1989; Dewing et al., 2007; Obermajer et al., 2007).

Permian–Triassic Biotic Changes

The marine invertebrate biota of the Sverdrup Basin underwent major changes during the Permian. Basin-margin sediments of Early Permian age (Sakmarian and younger) are dominantly cool-water carbonate ramp deposits composed of bryozoans, echinoderms, brachiopods, foraminifers, and solitary rugose corals with a minor fraction of sponge spicules (Beauchamp, 1989; Beauchamp and Desrochers, 1997; Beauchamp and Baud, 2002; Reid et al., 2007). Replacement of this prolific carbonate factory by a siliceous sponge-dominated biota occurred between the Artinskian (late Early Permian) and Guadalupian (late Middle Permian) as a consequence of climatic cooling and an increase in nutrient levels (Beauchamp and Henderson, 1994; Reid et al., 2007; Bensing et al., 2008).

The lower beds of the Upper Permian Lindström and Black Stripe Formations contain rare macrofaunal remains, but productid and spiriferid articulate brachiopods, trepostome and fenestrate bryozoans, and echinoderms all disappear near the base of the *Mesogondolella rosenkrantzi–Mesogondolella sheni* zone, around the lowest Changhsingian (Beauchamp, 1994; Henderson and Baud, 1997). Thereafter, fossil remains consist almost exclusively of siliceous sponge spicules (Gates et al., 2004). The spicules are 10–150 µm wide and 100–2000 µm long and include monactine monaxons and tetraxons, generally associated with the classes Demospongea and Hyalospongea, respectively (Rigby, 1987). The spicules were derived from sponges lacking a fused skeleton, and the resulting state of disaggregation makes generic identification impossible. The top of the *Mesogondolella sheni* zone, dating to the mid–late Changhsingian, marks the point where demosponges, hyalosponges, and some soft-bodied taxa (as noted by trace fossils) went extinct, culminating the progressive reduction in biodiversity that characterized the Middle to Late Permian of the Sverdrup Basin (Beauchamp, 1994). Since both sponge classes range from the Cambrian to the Holocene, their demise in the Sverdrup Basin during the Arctic extinction event represents either extinction at a lower taxonomic level or local rather than global taxonomic disappearances. Grasby and Beauchamp (2008, 2009) have correlated this extinction (Arctic extinction event) with the global mass extinction (latest Permian mass extinction), but this correlation is inaccurate because the succeeding *Clarkina hauschkei* zone represents a pre–latest Permian mass extinction level (see Biostratigraphic control section).

The basal 10–20 m of the Blind Fiord Formation (of latest Permian age) contain no biota except for microbes, rare ammodiscid foraminifers, and conodonts (Beauchamp and Baud, 2002) and exhibit very limited ichnofossil abundance (Beatty et al., 2008). The Griesbachian (earliest Triassic) is characterized by a limited macrofauna including several species of the ammonite genera *Otoceras*, *Ophiceras*, and *Bukkenites* and the bivalve *Claraia* (Henderson and Baud, 1997; Baud et al., 2008). Greater bioturbation is apparent from ~60 m above the base of the Blind Fiord Formation (Beatty et al., 2008), and a more diverse benthic macrofaunal assemblage that includes bryozoan biostromes is found in the Dienerian-Smithian, ~200–300 m above the Permian-Triassic boundary (Baud et al., 2008). However, sponges did not reappear in the Sverdrup Basin until the Middle Triassic.

STUDY SECTION

History of Investigation

The 24-m-thick study section at West Blind Fiord consists of the uppermost 6 m of the Lindström Formation and the lowermost 18 m of the Blind Fiord Formation (Fig. 2A). This section

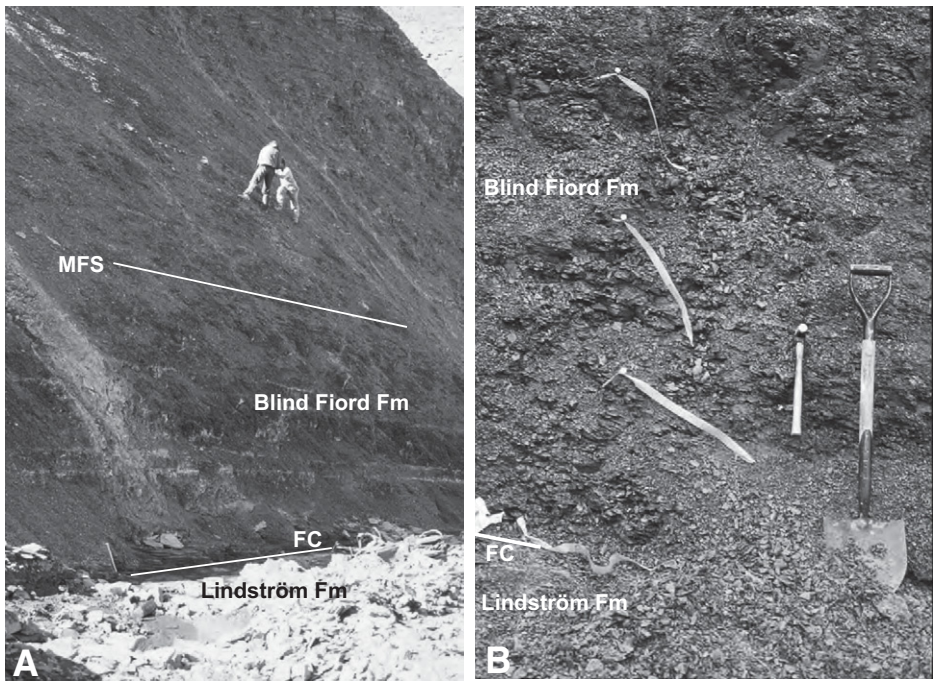

Figure 2. (A) West Blind Fiord section, Ellesmere Island. The formation contact (FC) marks the transition from spiculitic chert of the underlying Lindström Formation to nonspiculitic silty shale of the overlying Blind Fiord Formation; this horizon represents a regional extinction of sponges herein named the "Arctic extinction event." The maximum flooding surface is approximately correlative with the latest Permian extinction at Meishan D, and the Permian-Triassic boundary is near the position of the field geologists (Benoit Beauchamp and assistant Patti Harris). (B) Close-up of basal Blind Fiord Formation from which Late Permian species of *Clarkina* were recovered. Photos are by Charles Henderson.

was visited by Benoit Beauchamp and Charles Henderson first during the 1985 field season, when conodont samples were collected from the base of the Blind Fiord Formation (Fig. 2B). Beauchamp and Henderson revisited this section in 1989, when Henderson collected a larger suite of samples over a wider stratigraphic interval. The results of this biostratigraphic work were first reported at the Pangea meeting in Calgary (Henderson, 1993), when it was suggested that events in the Permian-Triassic boundary interval of the Canadian Arctic were diachronous with respect to the Tethyan Permian-Triassic boundary record. Subsequently, numerous additional sections were collected at sites on several Arctic islands by Beauchamp, Henderson, and co-workers, culminating in a summary paper by Beauchamp et al. (2009). Grasby and Beauchamp (2008, 2009) investigated the C-isotope stratigraphy and other geochemical signatures of a number of Arctic Permian-Triassic boundary sections, but these studies utilized the biostratigraphic framework of Beauchamp and Baud (2002) and did not fully integrate new biostratigraphic information developed by Henderson and reported in the present study (see next section).

Biostratigraphic Control

Research on conodont biostratigraphy of the Permian-Triassic boundary has advanced substantially in the past few years owing to studies in China (Jiang et al., 2007; Zhang et al., 2007; Chen et al., 2009) and Iran (Kozur, 2005; Shen and Mei, 2010). As a result of these studies, biostratigraphic age assignments and correlations of Tethyan and boreal conodont faunas now can be undertaken with greater confidence. A long-lived boreal *Mesogondolella* lineage, culminating in the Sverdrup Basin with *M. rosenkrantzi* and *M. sheni*, was replaced during the late Changhsingian by the *Clarkina* lineage, comparable to species and subspecies previously recognized only in the Tethyan region. Here, we document the occurrence of key conodont taxa at West Blind Fiord (Fig. 3) and show their relationship to the six conodont zones that have been identified in Permian-Triassic boundary sections from Ellesmere Island (Fig. 4; see also Henderson and Baud, 1997; Beauchamp et al., 2009).

M. rosenkrantzi–M. sheni Zone

This zone is defined by the co-occurrence of the two named taxa, which are the only conodonts present. *M. rosenkrantzi* (Figs. 3A and 3B) is a long-ranging, cool-water Lopingian (Wuchiapingian to Changhsingian) conodont species (Henderson and Baud, 1997; Mei et al., 1999; Mei and Henderson, 2001; Shen et al., 2010). Its co-occurrence with *M. sheni* suggests a lower to middle Changhsingian age. A similar succession occurs within the Fantasque Formation of northeastern British Columbia in western Canada (Henderson, 1997). At West Blind Fiord, this zone is located below the base of the present study section (Fig. 4A).

Mesogondolella sheni Zone

Specimens of *M. sheni* (Figs. 3C and 3D) from the TST at the base of Sequence 8 (upper Lindström Formation) indicate a Changhsingian age, but the exact relationship between these specimens and the type material from Selong, Tibet, which has been assigned to the late Changhsingian (Mei, 1996; Shen et al., 2006), still needs to be established. Integration with C-isotope records (see Carbon isotope correlations section) favors correlation of this zone with the upper *C. changxingensis* zone of late Changhsingian age. *M. sheni* represents the termination of the *Mesogondolella* lineage; it was replaced by immigrant species of *Clarkina* that had evolved in the Tethys during the Late Permian. At West Blind Fiord, this zone is represented by the lowermost 5.6 m of the study section, from its base to the level of datum B (= Arctic extinction event; Fig. 4A). Based on the age model presented in Age model and sedimentation rates, this zone has a minimum duration of ~100 k.y. (Fig. 4B).

Clarkina hauschkei Zone

This zone includes *Clarkina* cf. *changxingensis*, *Clarkina hauschkei*, *Clarkina* cf. *jolfensis*, and very rare *Hindeodus typicalis*. *Clarkina* cf. *changxingensis* (Figs. 3E, 3F, 3H, and 3I) represents a new subspecies of *C. changxingensis* similar to *C. yini* (Kozur, 2005); the latter was also described originally as a subspecies of *C. changxingensis* from Beds 23–24e at Meishan D (Yin et al., 2001). Our specimens of *C. hauschkei* (Figs. 3M and 3N) have been compared to those specimens described by Kozur (2005) as *Clarkina hauschkei borealis* from a zone below both the Permian-Triassic boundary clay and the microbialite facies at Abadeh, Iran. *Clarkina* cf. *jolfensis* (Figs. 3J and 3P) has the relatively large, posteriorly directed cusp of *Clarkina meishanensis*, but it has a fused carina that is more comparable to *C. jolfensis* from Iran. *Clarkina jolfensis* is associated with *C. yini* and *C. hauschkei* in Iran (Kozur, 2005). These three species all exhibit the flattening of the posterior platform, reduction in the width and depth of the adcarinal furrows, and a mostly small, posteriorly directed cusp that is typical of pre–latest Permian mass extinction conodonts of the *C. yini* zone of South China (Jiang et al., 2007; Zhang et al., 2007; Chen et al., 2009). At West Blind Fiord, this zone is represented by the interval from datum B (5.6 m) to datum C (9.0 m; Fig. 4A). Based on the age model of Age model and sedimentation rates, this zone has a duration of ~70 ± 10 k.y. (Fig. 4B).

Clarkina meishanensis Zone

Although *C. meishanensis* (Figs. 3G, 3K, and 3L) is restricted to Beds 25–28 at Meishan (Jiang et al., 2007), a similar species (*C. zhangi*) ranges from Bed 23 to Bed 24e. *C. zhangi* was originally described as a subspecies of *C. meishanensis* (Mei et al., 1998), and it is possible that these taxa represent the same species. *Clarkina meishanensis* migrated into Iran during the latest Changhsingian, correlative with Beds 23 and 24 at Meishan (Kozur, 2005), but its occurrence in various sections globally seems to be diachronous. This zone is interpreted to correlate with the *C. yini* and *C. meishanensis* zones of latest Changhsingian age, equivalent to Beds 24–27b at Meishan D (Henderson and Baud, 1997; cf. Chen et al., 2009). Associated species, at least in the lower part of the zone at Otto Fiord South (Fig. 4A), include *C. hauschkei* and *C.* cf. *changxingensis*, indicating an overlap with taxa characteristic of the *C. hauschkei* zone, a pattern also noted by Kozur (2005) from Iranian sections. Furthermore, Henderson and Baud (1997) reported the occurrence of the ammonoid *Otoceras concavum* within this zone, which has been accepted as a Late Permian species by Yin et al. (1996). At West Blind Fiord, this zone is represented by the interval from datum C (9.0 m) to datum E (= Permian-Triassic boundary, ~18 m; Fig. 4A). Based on the age model (see age model and sedimentation rates), this zone has a duration of ~140 ± 10 k.y. (Fig. 4B).

Clarkina taylorae–Hindeodus parvus Zone

Clarkina taylorae (Figs. 3Q and 3R) appears above the maximum flooding surface at Otto Fiord South closely associated with the ammonoid *Otoceras boreale*. Very rare specimens of *H. parvus* (Fig. 3O) appear a few meters higher in the same section (Henderson and Baud, 1997). The first occurrence of *C. taylorae* at its type locality in Selong, Tibet (Orchard et al., 1994), coincides with that of *H. parvus*, the first appearance datum (FAD) of which defines the Permian-Triassic boundary in the Meishan GSSP. Jiang et al. (2007) suggested that *C. taylorae* ranged below the Permian-Triassic boundary into Bed 27a at Meishan, but we interpret their figured specimens from Beds 27a and 27b as *C. zhejiangensis* and comparable to specimens referred to *C. praetaylorae* from Iran (Kozur, 2004; Chen et al., 2009). *Clarkina taylorae* represents a good index for the Permian-Triassic boundary when species of *Hindeodus* are rare; it has an upright cusp

and better developed adcarinal furrows that are typical of most immediately post–latest Permian mass extinction species of *Clarkina*. The stratigraphic position of the Permian-Triassic boundary was narrowly constrained at Otto Fiord South by the first appearances of *C. taylorae* and *H. parvus*, but this datum represents a local first occurrence (FO) of *H. parvus* that is younger than its FAD at Meishan. The correlative horizon at West Blind Fiord is ~13 m above the base of the Blind Fiord Formation. At West Blind Fiord, this zone approximately spans the uppermost 6 m of the study section (~18–24 m), between datums E and F (Fig. 4A). Based on the age model (see age model and sedimentation rates), this zone has a duration of ~70 ± 10 k.y. (Fig. 4B).

Clarkina taylorae–C. carinata Zone

Clarkina carinata (*Neogondolella* of some authors; for discussion, see Henderson and Mei, 2007) is the most commonly identified Lower Triassic conodont species (Clark, 1959; Sweet, 1970; Orchard and Krystyn, 1998). A sample from higher in the Blind Fiord Formation (~35 m above its base) yielded *C. taylorae*, *Clarkina tulongensis* (Fig. 3S), and *C. carinata* (Figs. 3T, 3U, 3V, and 3W), which are characteristic of the early Griesbachian (lowermost Triassic), equivalent to Beds 27c–30 at Meishan D (Jiang et al., 2007; Zhang et al., 2007; cf. Chen et al., 2009). Although conodont data are available only for these few horizons at West Blind Fiord, an age-equivalent section at Otto Fiord South on northern Ellesmere Island was the subject of a more detailed conodont study by Henderson and Baud (1997), and the two sections can be correlated accurately on the basis of C-isotope profiles (Grasby and Beauchamp, 2008) and sequence stratigraphic relationships (Beauchamp et al., 2009). At West Blind Fiord, this zone begins approximately at the top of the 24-m-thick study

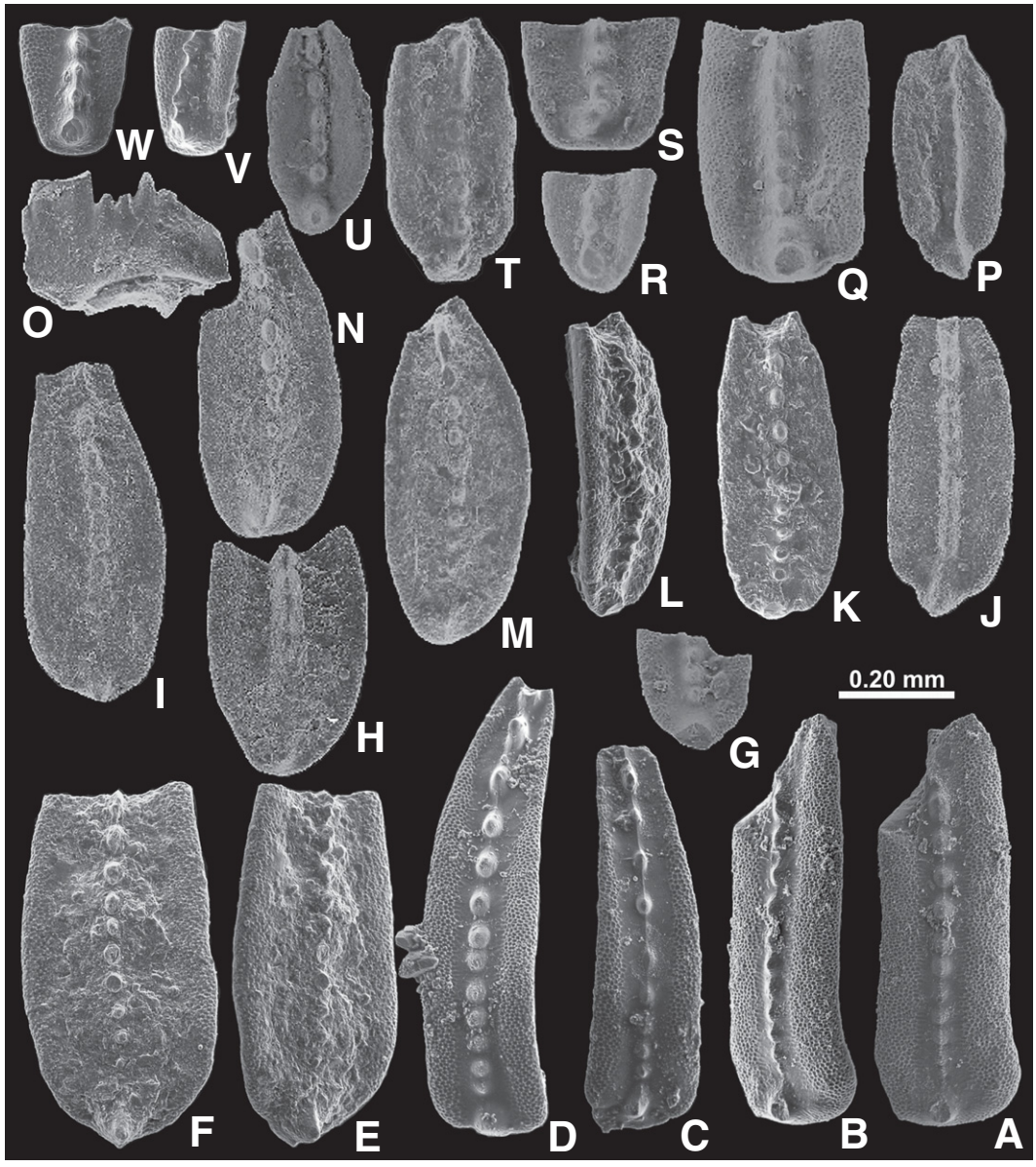

Figure 3. Scanning electron microscope (SEM) photomicrographs of conodonts from West Blind Fiord (WBF) and Otto Fiord South (OFS) sections. (A–B) *Mesogondolella rosenkrantzi*; WBF C-125990 (22 m below formation contact): (A) upper and (B) oblique upper view of same specimen. (C–D) *Mesogondolella sheni*: (C) WBF C-125990 (22 m below formation contact), upper view; and (D) WBF C-125991 (21 m below formation contact), upper view. (E–F, H–I) *Clarkina* cf. *changxingensis*; WBF C-125970 (0.2 m above formation contact): (E) oblique upper and (G) upper view of same specimen; (H–I) WBF C-125969 (0.1 m above formation contact), upper views. (G, K–L) *Clarkina meishanensis*; OFS (31.5 m above sequence boundary): (G) upper view; WBF C-125569 (50 m above formation contact), (K) upper and (L) oblique upper view of same specimen. (J, P) *Clarkina* cf. *jolfensis*: (J) WBF C-125969 (0.1 m above formation contact), upper view; and (P) WBF C-125970 (0.2 m above formation contact), upper view. (M–N) *Clarkina hauschkei*, WBF C-125969 (0.1 m above formation contact), upper views. (O) *Hindeodus parvus*, OFS (31.5 m above sequence boundary), lateral view. (Q–R) *Clarkina taylorae*, OFS (31.5 m above sequence boundary), upper views. (S) *Clarkina tulongensis*, OFS (31.5 m above sequence boundary), upper view. (T–W) *Clarkina carinata*, WBF C-125569 (50 m above formation contact): (T) upper view; (U) OFS (31.5 m above sequence boundary), upper view; (V–W) WBF C-125569 (50 m above formation contact), (V) oblique upper and (W) upper view of same specimen.

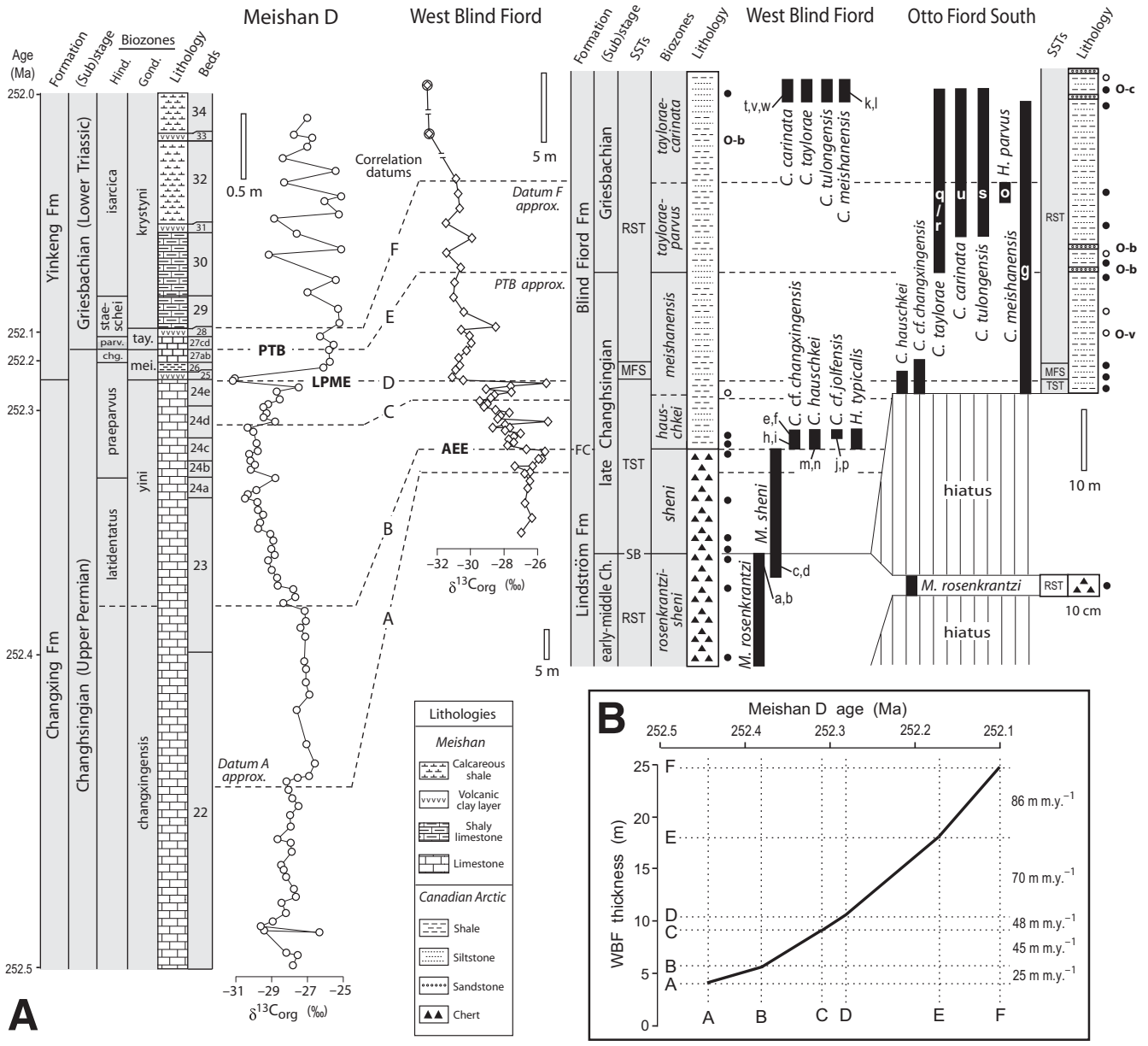

Figure 4. (A) Correlation of West Blind Fiord to Meishan D and Otto Fiord South based on biostratigraphic and $\delta^{13}C_{org}$ constraints. Datum B represents the Arctic extinction event (AEE), datum D is the latest Permian mass extinction (LPME), and datum E the Permian-Triassic boundary (PTB); the positions of datum A at Meishan and datums E and F at West Blind Fiord are approximate. For Meishan D, conodont zonation is from Jiang et al. (2007) and Zhang et al. (2007); $\delta^{13}C_{org}$ profile is from Cao et al. (2002); age model is based on Shen et al. (2010, 2011); note stratigraphic condensation in proximity to the Permian-Triassic boundary. For Otto Fiord South, conodont data are from Henderson and Baud (1997); correlations to West Blind Fiord were refined on the basis of C-isotope profiles in Grasby and Beauchamp (2008) and the sequence stratigraphic model of Beauchamp et al. (2009); note that the 10-cm-thick unit below the sequence boundary represents the feather edge of the Lindström Formation, which thins proximally. Abbreviations: SSTs—sequence systems tracts; MFS—maximum flooding surface; RST—regressive systems tract; SB—sequence boundary; TST—transgressive systems tract. For West Blind Fiord, conodont and $\delta^{13}C_{org}$ data are original to this study, except for uppermost two $\delta^{13}C_{org}$ points (circled; from Grasby and Beauchamp, 2008); note change in vertical scale at level of sequence boundary represented by the two 5 m scale bars. For both Canadian Arctic sections, productive samples and samples barren of conodonts are shown by solid and open dots, respectively, to right of lithologic columns; lowercase letters on or adjacent to biostratigraphic range bars refer to conodont specimens in Figure 3; note that *Clarkina hauschkei* and *C.* cf. *changxingensis* are equivalent, respectively, to *C.* cf. *subcarinata* and *C.* aff. *changxingensis* of Henderson and Baud (1997), and that *C.* cf. *changxingensis* is a new subspecies of *changxingensis* (C.M. Henderson). Abbreviations: Ch.—Changhsingian; chg.—*changxingensis*; gond.—gondollelids; hind.—hindeodids; mei.—*meishanensis*; parv.—*parvus*; tay.—*taylorae*. Recovery of ammonoids shown to right of lithologic columns: O-v—*Otoceras concavum*; O-b—*Otoceras boreale*; O-c—*Ophiceras commune*. (B) Sedimentation rate model for West Blind Fiord (WBF) based on an age model for the Meishan global stratotype section and point (GSSP; Shen et al., 2010) and correlation datums A–F of main figure; average sedimentation rates are shown at right.

section and includes stratigraphically younger beds analyzed by Grasby and Beauchamp (2008) and Beauchamp et al. (2009).

Carbon Isotope Correlations

Organic C-isotope records have utility for chemostratigraphic correlation, especially when biostratigraphically constrained (e.g., Gröcke, et al., 1999; Heimhofer et al., 2003; Weissert et al., 2008). Organic C-isotope profiles assisted in refining the correlations between West Blind Fiord and Meishan D already developed on the basis of conodont biostratigraphy (see Biostratigraphic control section). The two sections show similar patterns of variation in the precrisis interval of the Upper Permian. A gradual trend toward more ^{13}C-enriched values is observed in the upper *C. changxingensis* zone at Meishan, peaking in the upper Bed 22–lower Bed 23 interval (Cao et al., 2002), while a correlative shift is observed in the upper *M. sheni* zone at West Blind Fiord, peaking at the Lindström–Blind Fiord formation contact (Fig. 4A). Above the formation contact (= datum B), a sharp reversal initiated a trend toward more ^{13}C-depleted values that culminated at datum C within the *C. yini* zone (Bed 24) at Meishan and the *C. hauschkei* or lower *C. meishanensis* zone at West Blind Fiord. Between datums C and D, both sections show a gradual trend toward more ^{13}C-enriched values, a trend defined by eight samples over 0.3 m at Meishan and by six samples over 2.2 m at West Blind Fiord (and, thus, not a single-sample anomaly). At the level of datum D (= latest Permian mass extinction), both sections are characterized by a large (~4‰–5‰) and abrupt negative shift in $\delta^{13}C_{org}$ (Fig. 4A). The correlative character of the two organic C-isotope profiles breaks down above datum D, with Meishan showing relatively ^{13}C-enriched, but highly variable values and West Blind Fiord showing relatively ^{13}C-depleted and stable values.

The C-isotopic composition of organic matter is subject to global as well as local influences, and both may be apparent in the West Blind Fiord $\delta^{13}C_{org}$ profile (Fig. 5A). The pre–latest Permian mass extinction patterns exhibited by the sections at West Blind Fiord and Meishan are similar to those in other Permian-Triassic boundary sections globally, e.g., the Buchanan Lake section from the Sverdrup Basin (Grasby and Beauchamp, 2008; Fig. 5B), and the Trøndelag core from Norway (Hermann et al., 2010;

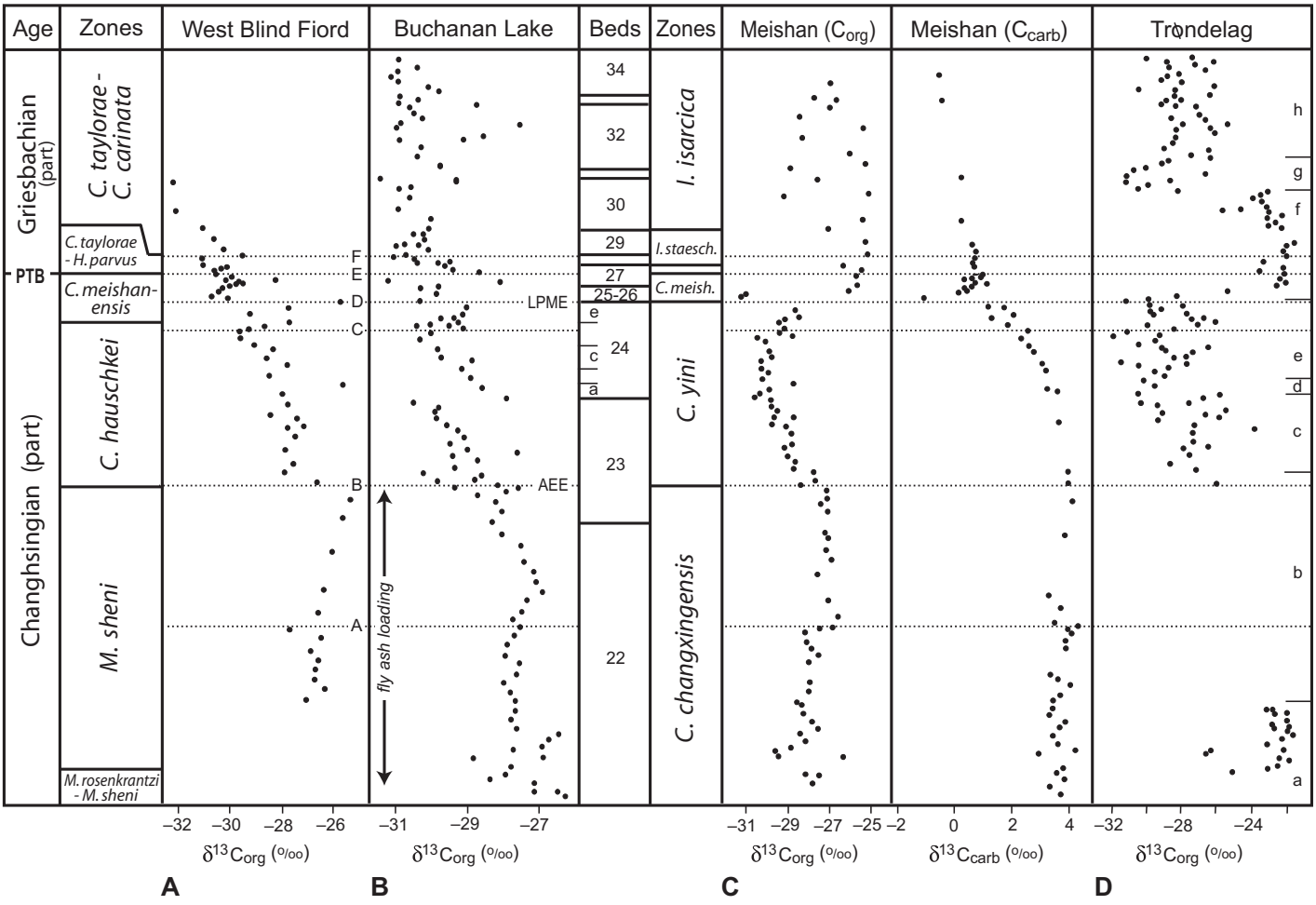

Figure 5. Comparison of organic C isotopic profiles for (A) West Blind Fiord (this study), (B) Buchanan Lake (Grasby and Beauchamp, 2008), (C) Meishan global stratotype section and point (GSSP; Cao et al., 2002; carbonate $\delta^{13}C$ profile also shown), and (D) Trøndelag core, Norway (Hermann et al., 2010). The Meishan profiles were plotted on a linear depth scale, and the other records were adjusted vertically within biostratigraphic constraints. The Arctic extinction event (AEE) coincides with the onset of a gradual negative shift at the base of Bed 23 in the Meishan C_{org} record, whereas the global latest Permian mass extinction (LPME) is located at a sharp negative-positive couplet at the base of Bed 25. The youngest interval of heavy fly ash deposition at Buchanan Lake (Grasby et al., 2011, their fig. 4) is indicated in B.

Fig. 5D). All four sections show a trend toward more ^{13}C-depleted values beginning around the *M. sheni*/*C. hauschkei* or *C. changxingensis*/*C. yini* zonal boundary (= datum B), followed by a reversal toward more ^{13}C-enriched values a little below the latest Permian mass extinction at datum C. These similarities suggest a common response at a global scale to carbon-cycle forcings, e.g., increased photosynthetic fractionation by eukaryotic marine plankton (as recorded by increasing $\Delta\delta^{13}C_{carb\text{-}org}$ at Meishan; Fig. 5C) in response to rising atmospheric CO_2 levels triggered by early-stage Siberian Traps volcanism. Above the latest Permian mass extinction (= datum D), the Trøndelag core exhibits a large and sustained shift toward more ^{13}C-enriched values similar to that at Meishan, whereas the Buchanan Lake section mirrors the lighter and more stable compositions shown by West Blind Fiord (Fig. 5). These divergent patterns may reflect regional differences in the degree to which marine primary production following the latest Permian mass extinction was taken over by prokaryotic green sulfur bacteria (Chlorobiaceae), which fractionate C isotopes during photosynthesis to a substantially smaller degree than eukaryotic algae and, hence, generate more ^{13}C-enriched organic matter (Riccardi et al., 2007). The inference of low abundances of green sulfur bacteria at West Blind Fiord based on light $\delta^{13}C_{org}$ values is confirmed by low concentrations of Chlorobiaceae-derived biomarkers (see Organic fraction section). Conversely, high abundances of green sulfur bacteria at Meishan are indicated both by heavy $\delta^{13}C_{org}$ values and by high concentrations of relevant biomarkers (Grice et al., 2005; Cao et al., 2009).

Marine carbonate C-isotope profiles of a specific age are often similar owing to the long residence time of dissolved inorganic carbon in seawater (~80 k.y.), which exerts a strong global influence. Carbonate $\delta^{13}C$ profiles for Permian-Triassic boundary sections can be readily correlated globally (e.g., Algeo et al., 2007; Tong et al., 2007; Luo et al., 2011). The Meishan $\delta^{13}C_{carb}$ profile is typical of these records, showing minor variation in the range of +3‰ to +4‰ through most of the Changhsingian, followed by a gradual –3‰ to –4‰ shift beginning in the mid–*C. yini* zone and culminating around the latest Permian mass extinction (Fig. 5C). Carbonate $\delta^{13}C$ records exhibit important differences in detail from organic $\delta^{13}C$ records, as shown by the paired profiles for Meishan (Cao et al., 2002). The onset of the negative shift in $\delta^{13}C_{carb}$ (= base of Bed 24 at Meishan) postdates that of the negative shift in $\delta^{13}C_{org}$ (= lower Bed 23 at Meishan) by an interval of ~100 k.y. (Fig. 4A). Further, the positive shift in the $\delta^{13}C_{org}$ profiles between datums C and D is not matched in $\delta^{13}C_{carb}$ profiles, in which the negative trend begun in the mid–*C. yini* zone continues to the level of the latest Permian mass extinction (Fig. 5C). Owing to such differences, correlations based on matching of $\delta^{13}C_{org}$ and $\delta^{13}C_{carb}$ profiles can result in erroneous inferences concerning temporal relationships. For example, Grasby and Beauchamp (2008, 2009) and Grasby et al. (2011) equated a negative shift in the $\delta^{13}C_{org}$ profiles of West Blind Fiord and Buchanan Lake (datum B) with the negative excursion in carbonate C-isotopes at the base of Bed 25 at Meishan. On this basis, Grasby and Beauchamp (2008) conflated the regional siliceous sponge extinction event represented by datum B (Arctic extinction event) with the global mass extinction event (latest Permian mass extinction) at Meishan and other Tethyan sections (datum D; Fig. 5). As discussed in Permian-Triassic biotic changes, the Arctic extinction event and latest Permian mass extinction are separate horizons in the Sverdrup Basin, and it is important to recognize them as such because this relationship reveals the globally diachronous character of the Late Permian biotic crisis.

Placement of Permian-Triassic Boundary, Latest Permian Mass Extinction, and Maximum Flooding Surface Horizons

The Permian-Triassic boundary was originally placed at the base of the Blind Fiord Formation (Nassichuk et al., 1973; Thorsteinsson, 1974), but recent definition of the Permian-Triassic boundary based on the FAD of the conodont *Hindeodus parvus* in the Meishan D GSSP (Yin et al., 2001) dictates a higher placement. The lowermost few meters of the Blind Fiord Formation have yielded the conodonts *C. hauschkei*, *C.* cf. *changxingensis*, and *C.* cf. *jolfensis* on the basis of which an uppermost Permian age has been inferred (Beauchamp et al., 2009). *H. parvus* was recovered 31.75 m above the base of the Blind Fiord Formation south of the head of Otto Fiord (Henderson and Baud, 1997), associated with the Early Triassic ammonoid *Otoceras boreale* and just below specimens of *Ophiceras commune*, although this horizon probably represents a local first occurrence of *H. parvus* rather than a true FAD. The stratigraphic correlation framework developed in this study (Fig. 4A) suggests that the Permian-Triassic boundary is ~13 m above the base of the Blind Fiord Formation at West Blind Fiord, with an uncertainty of about ±5 m.

The end-Permian mass extinction became the "latest Permian mass extinction" upon redefinition of the system boundary. In their analysis of the West Blind Fiord section, Grasby and Beauchamp (2008) placed the latest Permian mass extinction at the contact between the Lindström and Blind Fiord Formations (their fig. 4). However, we interpret the formation contact to represent a regional extinction event affecting the sponge biota of the Sverdrup Basin, herein termed the "Arctic extinction event" (see Introduction section). As shown by the correlation framework developed in Figures 4 and 5, the Arctic extinction event is ~5.6 m below the latest Permian mass extinction at West Blind Fiord and, hence, ~100 k.y. older than the latest Permian mass extinction as defined at Meishan D and elsewhere in the Tethyan region. At West Blind Fiord, the latest Permian mass extinction is located at ~10.2 m within a uniform interval of dark-gray shale lacking any macrofossils or trace fossils. This placement is supported by both biostratigraphic data and C-isotopic correlations (Figs. 4A and 5).

A maximum flooding surface represents the surface of maximum water depth in a given sequence and, thus, the transition from a transgressive systems tract (TST) to a highstand or regressive systems tract (RST) (Allen and Allen, 2005; Catuneanu et al., 2009). The maximum flooding surface of Sequence 8 of Beauchamp et al. (1989b) was assumed to be correlative with the Lindström–Blind Fiord Formation contact (FC) by Grasby and Beauchamp (2008, 2009). However, several features, including thinner bedding, increased total organic carbon (TOC) concentrations, and maxima in pyrite abundance and degree of pyritization values (see Organic fraction, and S-Fe system sections), suggest that the maximum flooding surface should be placed ~5 m above the formation contact at West Blind Fiord (Fig. 4A). Thus, the TST of Sequence 8 of Beauchamp et al. (1989b) extends through the lower ~5 m of the Blind Fiord Formation. The transition from the TST to the RST of Sequence 8 may have been due to an increasing influx of terrigenous detrital material resulting from elevated subaerial weathering rates during the Permian-Triassic boundary crisis interval (see Detrital fluxes and weathering rate changes section), rather than from a fall in global sea-level elevations. In fact, eustatic elevations probably continued to rise into the Early Triassic due to climatic warming (Hallam and Wignall, 1999), so the RST of Sequence 8 at West Blind Fiord is likely to represent the point in time at which rates of sediment influx into the Sverdrup Basin outpaced rates of eustatic deepening.

Age Model and Sedimentation Rates

We constructed an age model for the West Blind Fiord section (Fig. 4B) based on the correlation framework developed previously herein (see Biostratigraphic control, and Carbon iso-

tope correlations sections; Fig. 4A) in combination with a recent high-resolution radiometric time scale for the Late Permian (Shen et al., 2010, 2011). This new time scale, based on isotope dilution–thermal ionization mass spectrometry (ID-TIMS) U-Pb dating of zircons from South China Permian-Triassic boundary sections, provides multiple age tie points: key tie points (referenced to the Meishan GSSP) include the Bed 21-22 boundary (252.50 ± 0.11 Ma) and the Bed 25 (252.28 ± 0.08 Ma) and Bed 28 ash layers (252.10 ± 0.06 Ma), with an interpolated age of 252.17 ± 0.06 Ma for the Permian-Triassic boundary. Although sedimentation rates at Meishan were high during most of the Early Triassic (Algeo and Twitchett, 2010, their fig. 1), this section is marked by strong stratigraphic condensation around the Permian-Triassic boundary (Bowring et al., 1998); specifically, Beds 25–28 accumulated at approximately one-tenth the rate of underlying and overlying beds (Fig. 4A). Such section-specific, time-dependent changes in sedimentation rates are the source of nonlinearities in the correlation framework between the West Blind Fiord and Meishan sections (see datums A–F; Fig. 4A).

Correlation of West Blind Fiord to the Meishan GSSP allowed estimation of sedimentation rates and the durations of specific stratigraphic intervals within the study section. The 10.2 m section at West Blind Fiord below the latest Permian mass extinction (equivalent to Meishan beds 22–24e) accumulated at rates of ~25–48 m m.y.$^{-1}$ and represents an interval of ~300 k.y. (Fig. 4B). The ~8 m section between the latest Permian mass extinction and the Permian-Triassic boundary (equivalent to Meishan beds 25–27b) accumulated at a rate of ~70 m m.y.$^{-1}$ and represents ~110 k.y. The 6 m section immediately overlying the Permian-Triassic boundary (equivalent to Meishan beds 27c–28) accumulated at a rate of ~86 m m.y.$^{-1}$ and represents an interval of only ~70 k.y. Thus, sedimentation rates at West Blind Fiord increased more-or-less continuously through the Permian-Triassic boundary interval, with the largest stepwise increase (80%, i.e., from 25 to 45 m m.y.$^{-1}$) occurring at the formation contact (datum B; Fig. 4B). An increase in sedimentation rates within the Permian-Triassic boundary interval has been observed widely in the Sverdrup and Western Canadian basins (e.g., Hays et al., 2007; Beauchamp et al., 2009).

RESULTS

Detrital Siliciclastic Fraction

In total, 56 samples from the 24-m-thick West Blind Fiord section were analyzed in the present study (see Methods supplement for details of preparatory and analytical procedures[1]). The formation contact at 5.6 m is marked by abrupt shifts in major-element concentrations associated with the detrital fraction but relatively smaller changes in trace elements. The upper part of the Lindström Formation (0–5.6 m at West Blind Fiord) contains abundant SiO_2 (80%–90%) but only limited Al_2O_3 (2%–4%) and K (<0.5%; Figs. 6A–6C). The silica is present mainly as chert derived from siliceous sponges and, hence, is of biogenic origin (Beauchamp and Desrochers, 1997; Beauchamp and Baud, 2002). Al is present mainly in the clay fraction, in which the dominant mineral is chlorite (Fig. 7A). The overlying Blind Fiord Formation (5.6–24 m at West Blind Fiord) contains smaller quantities of SiO_2 (50%–60%) but larger amounts of Al_2O_3 (15%–18%) and K (3%–4%; Figs. 6A–6C). The latter elements reside mainly in the clay fraction, whereas silica is present both in the clay fraction and as quartz silt. Major minerals in the clay fraction include illite, illite/smectite, and chlorite (Figs. 7B–7D). Trace metals (Figs. 6D–6F) exhibit concentrations that are mostly close to those of post-Archean average shale (PAAS; Taylor and McLennan, 1995), suggesting residence primarily in the detrital fraction. Although V is somewhat enriched relative to PAAS in the Blind Fiord Formation, strong covariance with Al and K indicates residence mainly in the detrital fraction. In contrast, Mo shows local enrichments, especially between datum A (4.0 m) and the formation contact (5.6 m), which may represent a redox control (see Paleoredox conditions and environmental changes section). Other components of the sediment, such as calcite, organic matter, and pyrite, are present in only small quantities (<5%).

The chemical index of alteration (CIA) is a commonly used proxy for the degree of weathering of siliciclastic sediments, with higher values signifying more intense weathering (Nesbitt and Young, 1982; Price and Velbel, 2003). This ratio generally reflects the extent of conversion of feldspars to clay minerals, especially cation-poor clays such as kaolinite (Maynard, 1992; Sutton and Maynard, 1993). In the Lindström Formation, CIA values decrease from 0.65 to 0.70 at the base of the section to 0.50–0.55 just below datum A at 4.0 m (Fig. 6G). CIA values then rise sharply to >0.80 and remain generally high to the formation contact at 5.6 m. CIA values fall abruptly to ~0.72 at the base of the Blind Fiord Formation and then decline gradually to ~0.62 toward the top of the section but without a measurable shift at the latest Permian mass extinction horizon.

Cross plots of high field strength elements (e.g., Nb/Y vs. Zr/Ti) were devised to discriminate among magma types (Winchester and Floyd, 1977; Pearce, 1996), but they have also been employed to assess the provenance of siliciclastic sediments (Umazano et al., 2009). At West Blind Fiord, the lower part of the Lindström Formation (0–4.0 m) exhibits the lowest Nb/Y and the highest Zr/Ti ratios, whereas the upper Lindström Formation (4.0–5.6 m) exhibits a shift toward higher Nb/Y and lower Zr/Ti ratios (Fig. 8). All Lindström Formation samples plot within the field of rhyodacite to dacite magmas, suggesting derivation from source rocks of intermediate to slightly felsic composition, a pattern typical of coarser siliciclastics derived from old cratons (cf. Fralick, 2003). Samples of the Blind Fiord Formation plot mostly within the field of PAAS, indicating a mixed provenance, as is typical of shales. This graph reveals a systematic up-section change in the composition of the detrital fraction beginning at datum A (4.0 m) in the upper Lindström Formation—a change that is not apparent in the major- and trace-element profiles of Figure 6.

Major-element concentration data can be used to estimate the concentrations and fluxes of the major mineral fractions, including clay minerals, detrital quartz, biogenic chert, and calcite (see Methods supplement [see footnote 1]). The upper part of the Lindström Formation (0–5.6 m at West Blind Fiord) consists of 15%–30% clay minerals and detrital quartz, 70%–85% biogenic chert, and <2% calcite (Fig. 9A). The mineral-fraction composition of samples changed abruptly at the formation contact, and the overlying Blind Fiord Formation (5.6–24 m at West Blind Fiord) generally consists of ~80% clay minerals, 16%–18% detrital quartz, 2%–4% calcite, and 0% biogenic chert. A few samples (at 7 m, 14 m, and 22–23 m) contain larger amounts of calcite (to 9%) and measurable concentrations of "biogenic" silica (Fig. 9A); however, these samples were identified as siltstones in the field and are likely to have a higher silt:clay ratio than that used in estimating detrital quartz concentrations (see Methods supplement [see footnote 1]); hence, all of the quartz/chert in these samples is presumed to be of detrital origin. Mineral-fraction fluxes also changed abruptly at the formation contact (Fig. 9B). The flux of biogenic chert decreased from ~5 g cm^{-2} k.y.$^{-1}$ in the Lindström Formation to ~0 g cm^{-2} k.y.$^{-1}$ in the Blind Fiord Formation, while the flux of clay minerals and detrital quartz increased from <0.5 g cm^{-2} k.y.$^{-1}$

[1]GSA Data Repository item 2012072, Tables containing elemental, isotopic, and biomarker data for West Blind Fiord section, is available at http://www.geosociety.org/pubs/ft2012.htm or by request to editing@geosociety.org.

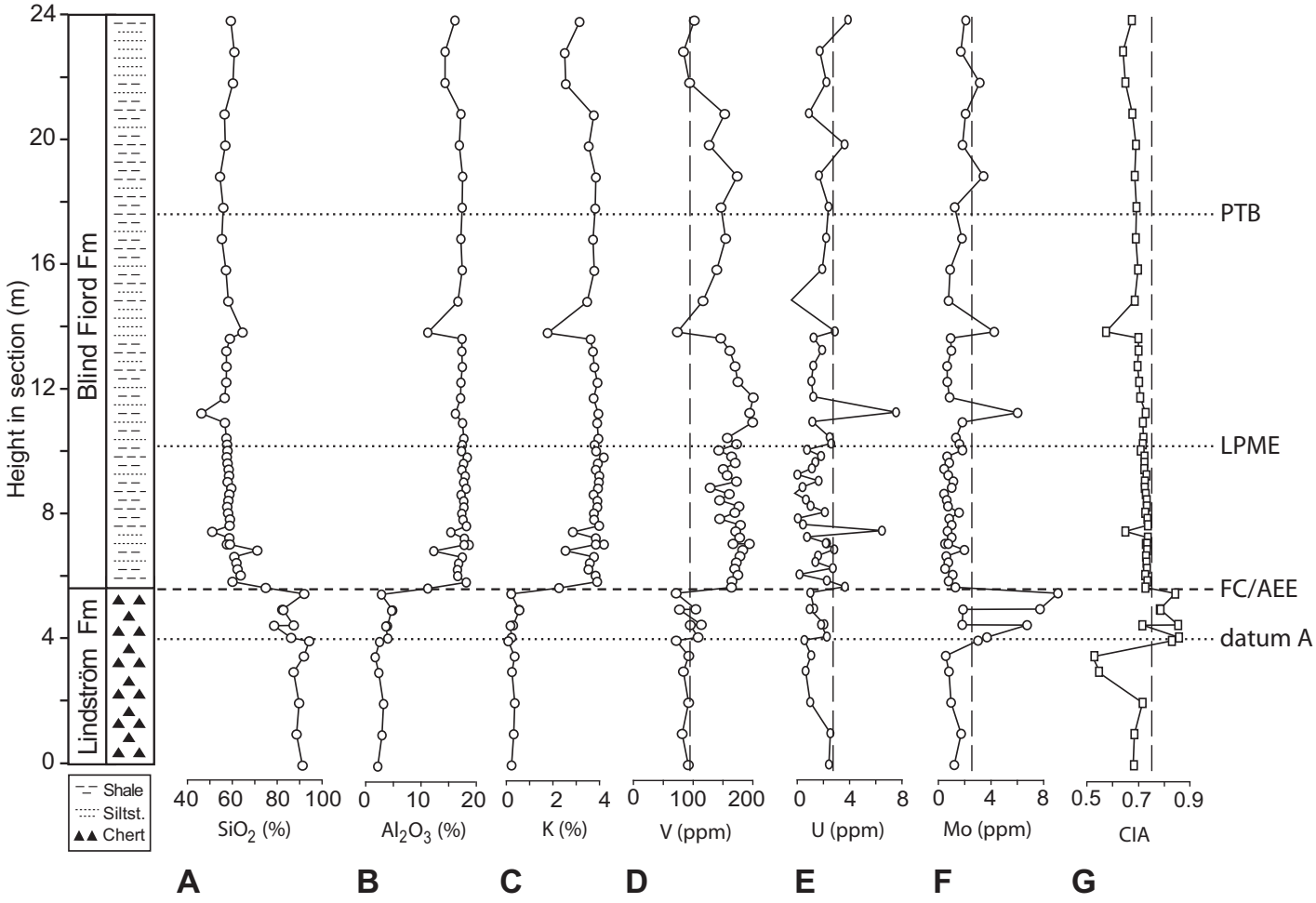

Figure 6. Chemostratigraphy (detrital fraction): (A) SiO_2, (B) Al_2O_3, (C) K, (D) V, (E) U, (F) Mo, and (G) CIA (chemical index of alteration). CIA is calculated as $Al_2O_3/(Al_2O_3 + K_2O + Na_2O + CaO_{noncarb})$ (Eq. 1 of Methods supplement [see text footnote 1]). The dashed vertical lines in columns D–F represent the composition of post-Archean average shale (PAAS; Taylor and McLennan, 1995); the dashed line in column G is intended only to assist with recognition of vertical trends. Abbreviations: AEE—Arctic extinction event; FC—formation contact; LPME—latest Permian mass extinction; PTB—Permian-Triassic boundary.

to >10 g cm^{-2} $k.y.^{-1}$ Thus, the bulk sediment flux of the Lindström Formation (~6 g cm^{-2} $k.y.^{-1}$) was dominated by biogenic silica, whereas that of the Blind Fiord Formation (~12–21 g cm^{-2} $k.y.^{-1}$) was dominated by detrital components (Fig. 9B). Bulk sediment flux is directly proportional to linear sedimentation rate, changes in which occur at stratigraphic levels corresponding to age tie points in our correlation framework (Fig. 4B). Thus, the stepwise increases in bulk sediment flux shown in Figure 9B may be a procedural artifact. In view of the relatively continuous increase in sedimentation rates at West Blind Fiord during the latest Permian (Fig. 4B), it is reasonable to infer that bulk sediment flux accelerated at the formation contact and thereafter increased steadily during deposition of the Blind Fiord Formation (heavy dashed line, Fig. 9B).

Organic Fraction

TOC values are low (0.2%–0.5%) throughout the study section but show a distinct pattern of stratigraphic variation (Fig. 10A). TOC increases sharply at datum A, peaking at 0.5%, and then falls toward the latest Permian mass extinction interval. Above the latest Permian mass extinction (10.2 m), TOC remains relatively elevated (0.4%–0.5%) to near the top of the study section. Biomarkers confirm the presence of thermally mature marine organic matter in all samples, as shown by C_{31}/C_{30} hopane ratios of 0.26–0.53 and C_{22}/C_{21}, C_{24}/C_{23}, and C_{26}/C_{25} tricyclic ratios of 0.15–0.30, 0.25–0.60, and 0.65–1.05, respectively (cf. Peters et al., 2004). However, these compounds do not provide any information regarding the presence or absence of highly weathered (and thus relatively inert) terrestrial organic matter. A petrographic study revealed considerable amounts of organic matter of both marine and terrestrial provenance in two samples close to the formation contact (Fig. 11). Clumps of marine organic matter tend to be larger than terrestrial fragments of vitrinite and inertinite, so the former probably dominates volumetrically. The absence of a relationship between clay content (Fig. 9A) and TOC (Fig. 10A) is noteworthy, indicating that grain-size variation did not serve as a dominant control on organic-matter accumulation (cf. Kennedy et al., 2002). More generally, changes in the C-N-S proxies at West Blind Fiord are largely independent of lithologic changes (which are confined mainly to the formation contact at 5.6 m), indicating that the former provide a record of biogeochemical influences in the West Blind Fiord depositional system rather than of lithologic controls.

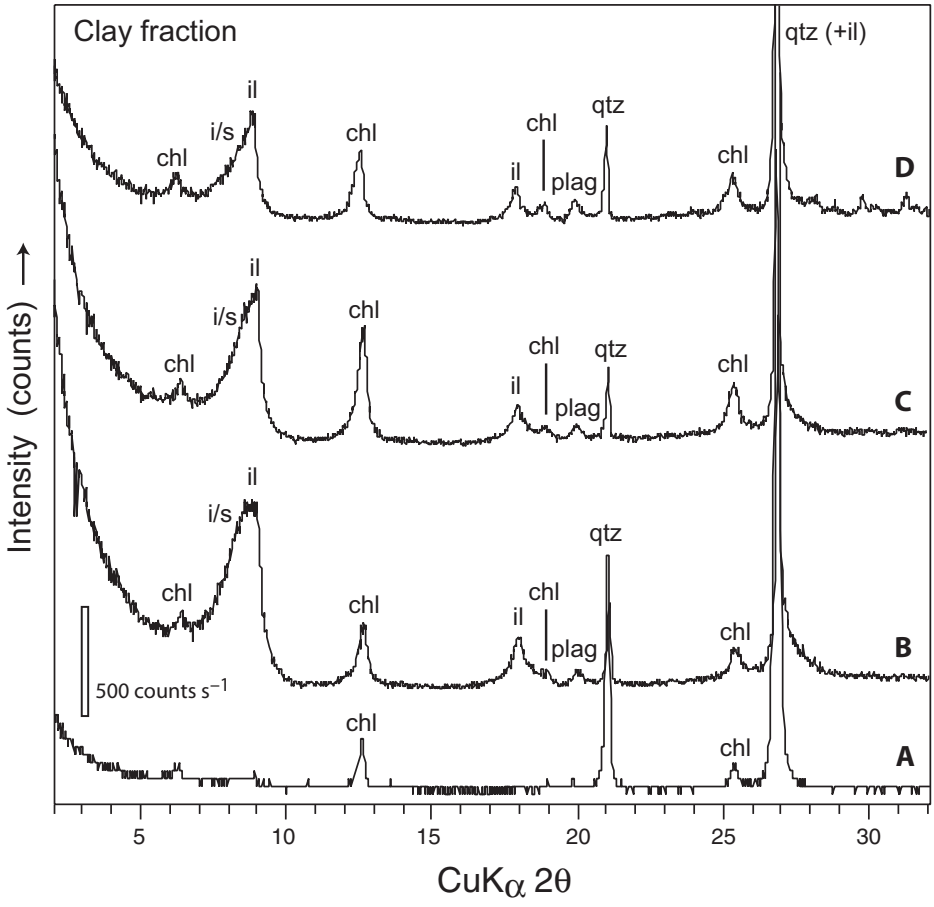

Figure 7. X-ray diffraction (XRD) traces of clay fractions for (A) WBF-354 (2.0 m), (B) WBF-305 (6.1 m), (C) WBF-310 (7.1 m), and (D) WBF-341 (19.9 m). A is from the Lindström Formation; B–D are from the Blind Fiord Formation. Abbreviations: chl—chlorite, il—illite, i/s—mixed-layer illite/smectite, plag—plagioclase, and qtz—quartz. Note that quartz peaks represent both detrital quartz and authigenic chert.

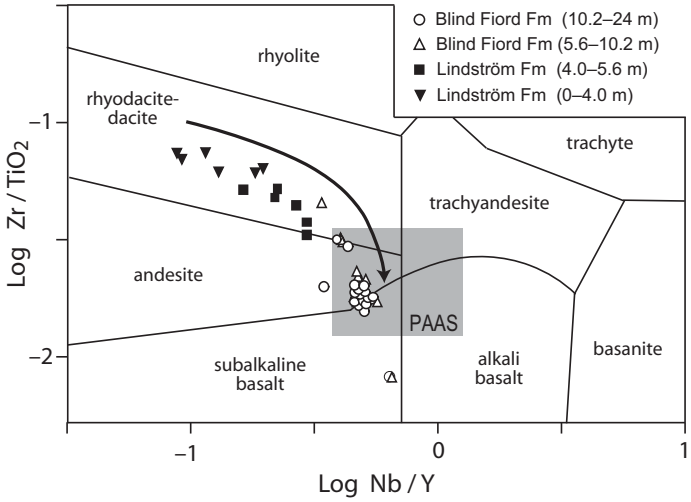

Figure 8. Discriminant plot of high field strength elements: Zr/Ti versus Nb/Y. Arrow indicates vector of chemical evolution of West Blind Fiord samples proceeding up section. Magmatic fields are from Pearce (1996); post-Archean average shale (PAAS) compositional field is from Taylor and McLennan (1995).

Organic carbon $\delta^{13}C$ values are between –26‰ and –27‰ below datum A (0–4.0 m), but they show a slight shift toward more ^{13}C-enriched values (–25‰ to –26‰) between datum A and the formation contact (Fig. 10B). The $\delta^{13}C_{org}$ profile shifts abruptly toward more negative values at the formation contact (5.6 m) and then exhibits a gradual negative trend (from –27.5‰ to –29.5‰) as the latest Permian mass extinction horizon is approached. At the latest Permian mass extinction horizon (10.2 m), the profile shows an abrupt excursion toward a heavier composition (–25.5‰), followed by an equally rapid shift toward lighter values (–30‰ to –32‰), which are sustained to the top of the section. N isotopes are mostly +4.0‰ to +5.0‰ below datum A (0–4 m), but they shift toward heavier values (+4.8‰ to +5.7‰) between datum A and the formation contact (Fig. 10C). Just below the formation contact (5.6 m), the N isotope profile shows an abrupt excursion toward a lighter composition (+2.3‰), followed by a shift toward heavier values (+5.5‰ to +6.5‰) between the formation contact and the latest Permian mass extinction horizon. Above the latest Permian mass extinction (10.2 m), the N isotope profile exhibits a shift back toward lighter values (+4.5‰ to +5.2‰), which remain relatively uniform to the top of the section.

The concentration profiles of all biomarkers measured in the West Blind Fiord section fluctuate over relatively narrow ranges. Aryl isoprenoids (AI) are present in all samples analyzed, although at relatively low concentrations (<12 ng/g TOC; Fig. 10D). AIs increase gradually upward throughout the 24-m-thick section but show a local maximum in the 2 m interval just below the latest Permian mass extinction. The ratio of 28,30-dinorhopane (DNH) to C_{30} hopane (28,30-DNH ratio) ranges from 0.15 to 0.65, with higher values above the formation contact (Fig. 10E). The C_{27}/C_{29} sterane ratio shows a similar pattern, ranging between 0.6 and 1.2, with higher values above the formation contact (Fig. 10F). Both the 28,30-DNH and C_{27}/C_{29} sterane ratios show small, transient decreases at the latest Permian mass extinction horizon (10.2 m). The 2-methylhopane index (2-MeHI), i.e., the ratio of 2-methylhopane to (2-methylhopane + hopane), shows generally higher values below the formation contact (mostly 2%–5%) and lower values above the formation contact (mostly <2%; Fig. 10G), but the range of values is muted. The homohopane index (HHI), i.e., the ratio of C_{35} to C_{34} homohopanes (Peters et al., 2004), also shows little variation (0.5–0.9), except for a peak (2.7) at the latest Permian mass extinction (Fig. 10H). The Ts/(Ts + Tm) profile, which is the ratio of two

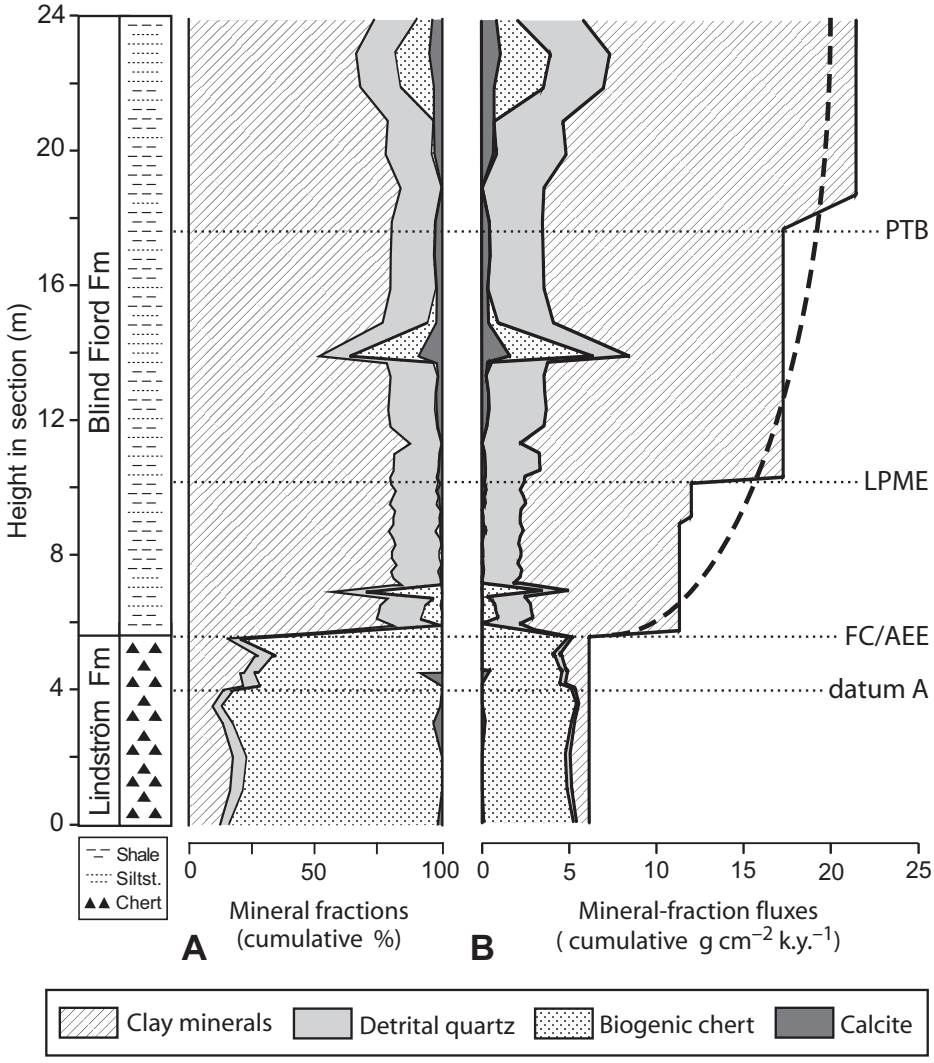

Figure 9. Stratigraphic trends in (A) mineral fractions and (B) mineral-fraction fluxes. Values in both panels are cumulative. Mineral fractions were calculated per Equations 2–6 and fluxes per Equations 7–8 of Methods supplement (see text footnote 1). Bulk (total) sediment flux is given by the rightmost solid curve in B; the stepped character of this curve is a function of assuming constant linear sedimentation rates between age tie points in Figure 4B. Abbreviations: AEE—Arctic extinction event; FC—formation contact; LPME—latest Permian mass extinction; PTB—Permian-Triassic boundary.

C_{27} hopanes, shows a limited range (0.64–0.67) through most of the study section but modestly lower values below datum A (Fig. 10J). The Ts/(Ts + Tm) ratio commonly varies as a function of organic source, sediment lithology, and thermal maturity (Moldowan et al., 1986); relatively uniform values in the West Blind Fiord section may reflect the similar maturity of all samples. The indigenous character of the biomarkers to the host rock is confirmed by parallel changes in multiple biomarkers in concert with other geochemical proxies, as well as by the observation that multiple parameters for source rock depositional facies change in conjunction with the lithologic transition from chert to shale at the formation contact. The generally low abundances of AI and other biomarkers, as well as the carbon-number distributions in the samples, are consistent with the intermediate level of thermal maturity of the study area (see Basinal sequence stratigraphy section).

Cross plots of TOC versus TN (Fig. 12A) and $\delta^{13}C_{org}$ versus $\delta^{15}N$ (Fig. 12B) reveal marked changes in the composition of the organic fraction with stratigraphic position. In both cross plots, sample groups for the Lindström (0–5.6 m), lower Blind Fiord (5.6–10.2 m), and upper Blind Fiord formations (10.2–24 m) show little overlap, and the differences in sample population means are highly significant ($p[\alpha] < 0.001$). Lindström Formation samples yield C_{org}:N ratios of ~20–30, $\delta^{13}C_{org}$ values of –25.5‰ to –27.5‰, and $\delta^{15}N$ values of +4.0‰ to +5.8‰. Blind Fiord Formation samples yield uniformly lower C_{org}:N ratios (mostly 2–5) and almost uniformly lower $\delta^{13}C_{org}$ values (mostly –27.0‰ to –29.5‰). Although lower and upper Blind Fiord samples exhibit similar C_{org}:N ratios (Fig. 12A), these two groups are readily distinguished on the basis of $\delta^{13}C_{org}$ and $\delta^{15}N$ values (Fig. 12B). Upper Blind Fiord samples yield more ^{13}C-depleted (–30.0‰ to –31.7‰) and ^{15}N-depleted (+4.5‰ to +5.3‰) compositions relative to the $\delta^{13}C_{org}$ (–27‰ to –30‰) and $\delta^{15}N$ (+5.1‰ to +6.4‰) compositions of lower Blind Fiord samples.

S-Fe System

Total sulfur (S) concentrations in the Lindström Formation are uniformly low (<0.2%) below datum A (4.0 m) but rise to somewhat higher values (0.5%–0.6%) between datum A and the formation contact (4.0–5.6 m; Fig. 13A). Total S concentrations in the Blind Fiord Formation are uniformly low (<0.2%) between the formation contact and the latest Permian mass extinction (5.6–10.2 m) but rise to substantially higher values (mostly >1.0%) above the latest Permian mass extinction horizon (10.2 m). More than 95% of total S is pyrite S (data not shown), and most of this S (especially in the high-S intervals) is "excess S" (Fig. 13A), i.e., S that exceeds the amount of reduced S expected relative to TOC for oxic-suboxic marine facies (Berner and Raiswell, 1983; Leventhal, 1983). Petrographic study showed that pyrite was present both as irregular masses and framboids, and that pyrite was associated almost exclusively with organic clumps of probable marine origin (Fig. 11). In contrast, organic macerals of undoubted terrestrial provenance show virtually no pyrite overgrowths.

A TOC-S cross plot reveals that Lindström Formation samples from below datum A (0–4.0 m) and Blind Fiord samples from between the formation contact and latest Permian mass extinction horizon (5.6–10.2 m) cluster along the oxic-suboxic marine trend of Berner and Raiswell (1983; Fig. 14). Lindström Formation samples from between datum A and the formation contact (4.0–5.6 m) define a vector toward higher S concentrations relative to TOC (trend 1), and Blind Fiord Formation samples from above the latest Permian mass extinction (10.2–24 m) define a second vector toward higher S concentrations relative to TOC (trend 2). These trends reflect increasing

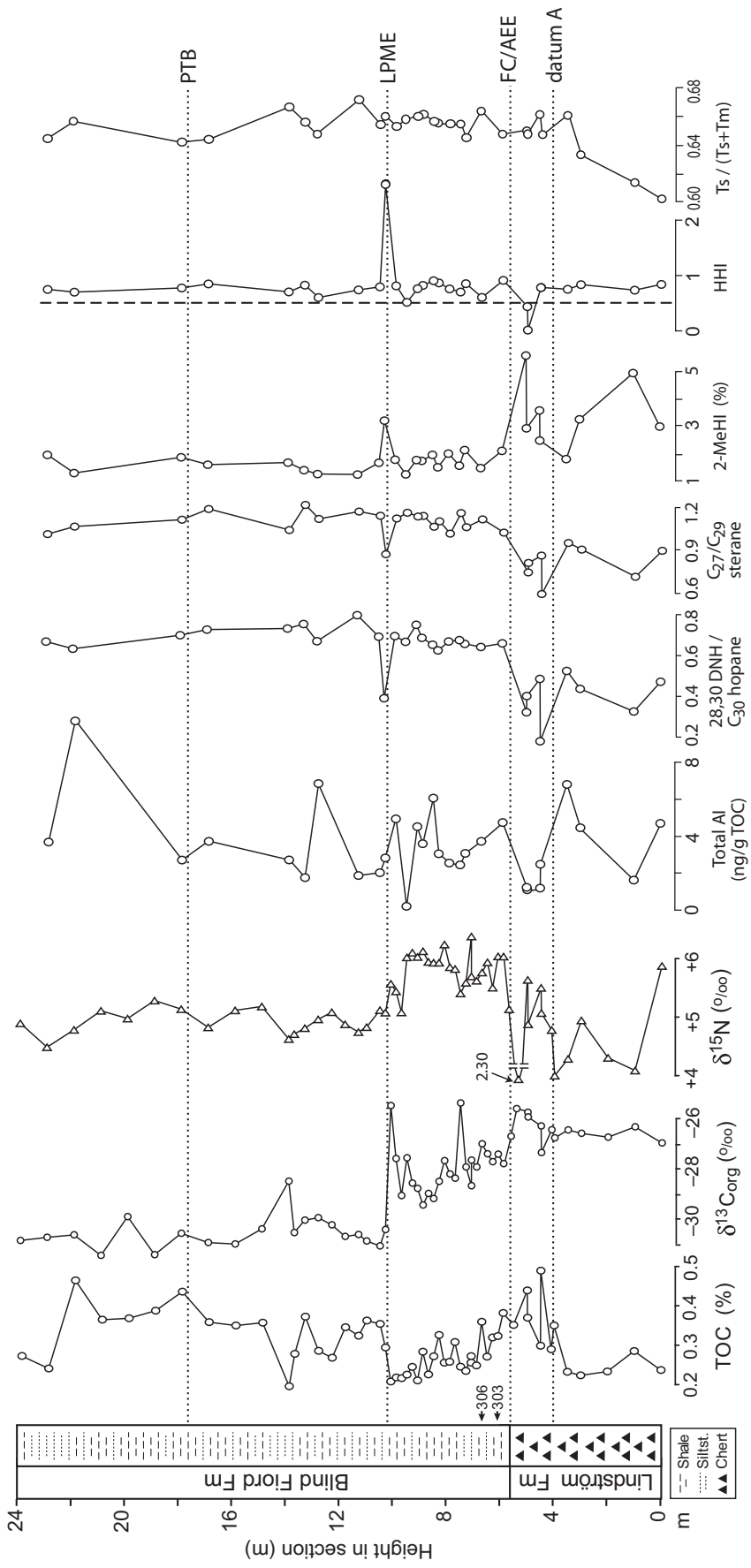

Figure 10. Chemostratigraphy (organic fraction): (A) total organic carbon (TOC), (B) $\delta^{13}C_{org}$, (C) $\delta^{15}N$, (D) total AI (aryl isoprenoids), (E) 28,30 dinorhopane (DNH) ratio, (F) C_{27}/C_{29} sterane ratio, (G) 2-MeHI (methylhopane index), (H) HHI (homohopane index), and (I) Ts/(Ts + Tm) ratio. In H, values >0.5 (dashed vertical line) are indicative of anoxic conditions (Peters et al., 2004). The positions of samples WBF-303 and WBF-306 used in petrographic analysis (Fig. 11) are shown to right of lithologic column. Abbreviations: AEE—Arctic extinction event; FC—formation contact; LPME—latest Permian mass extinction; PTB—Permian-Triassic boundary.

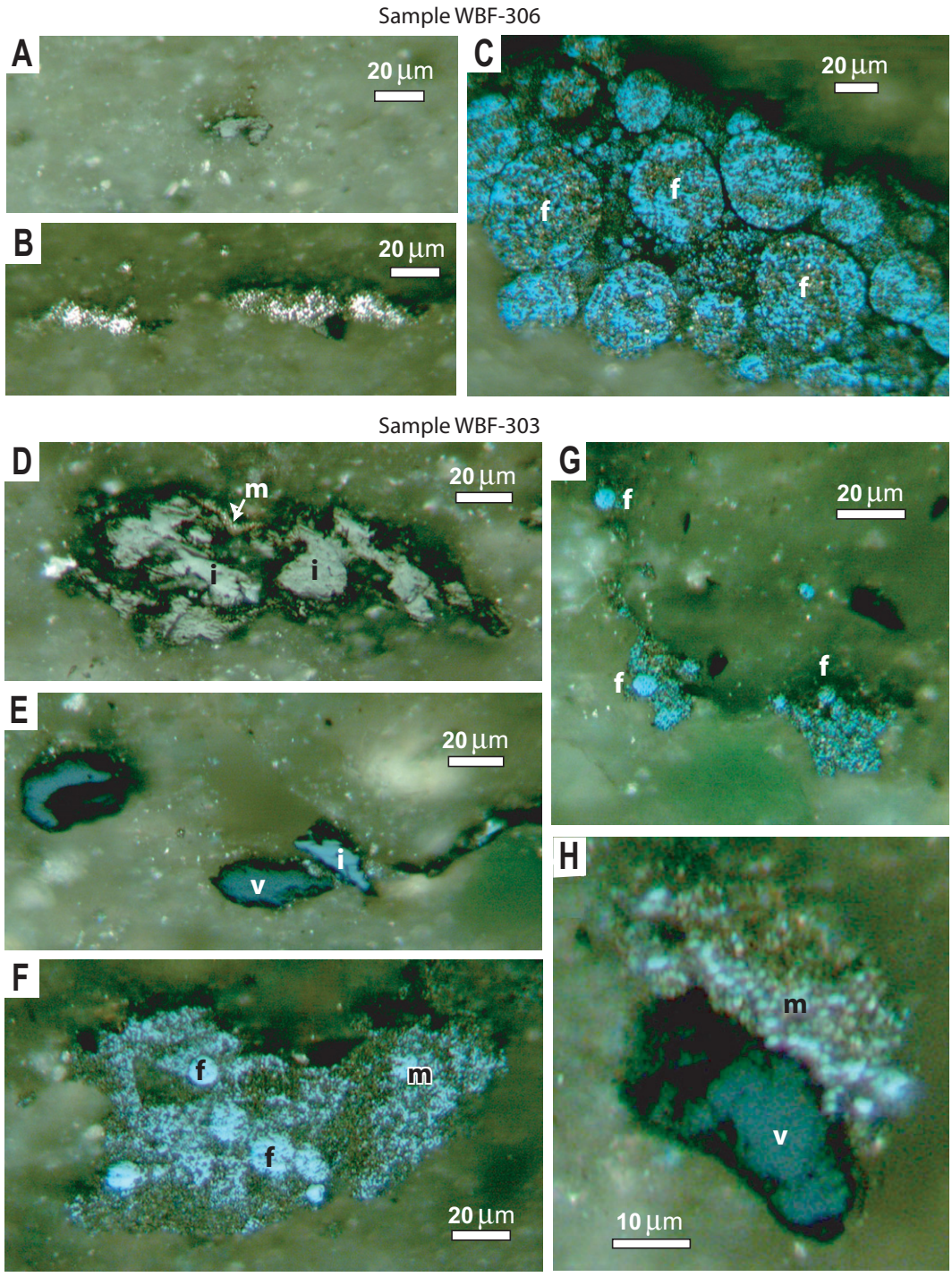

Figure 11. Photomicrographs: (A–C) sample WBF-306, (D–H) sample WBF-303. Vitrinitic (v) and inertinitic (i) macerals of probable terrestrial origin are seen in A, D–E, and H; these organic fragments exhibit few pyrite overgrowths owing to their relatively refractory character. Organic matter of probable marine origin (possibly in the form of fecal pellets) is seen in B–C and F–H; these organic clumps show nearly complete pyrite overgrowths owing to their labile character, which favors bacterial sulfate reduction. Pyrite is present both as irregular masses (m) and as framboids (f), the smaller of which (≤5 µm; e.g., in G) may have formed syngenetically in the water column, and the larger of which (>5 µm; e.g., in C) formed either partly or entirely within the sediment.

amounts of excess S (see previous) that may be related to the accumulation of syngenetic pyrite in the sediment. The observation that excess S increases with higher TOC may have significant implications for the relationship between paleoredox conditions and marine productivity (see Paleoredox conditions and environmental changes, and Plankton community and changes in primary productivity sections).

Degree of pyritization is a commonly used paleoredox proxy that represents the ratio of pyrite Fe to total reactive Fe (i.e., pyrite Fe plus extractable Fe that is potentially pyritizable; Raiswell et al., 1988). Degree of pyritization values are low (<0.2) in the lower part of the study section but increase abruptly at the latest Permian mass extinction horizon (10.2 m) to 0.40–0.45 (Fig. 13B). Degree of pyritization values fluctuate above the latest Permian mass extinction but episodically reach values >0.2 through the remainder of the section. Total Fe concentrations, ranging from 2% to 8%, yield a profile quite similar to magnetic susceptibility: low values below datum A, a transient rise between datum A and the formation contact, a sustained rise above the formation contact and peaking at ~7.5 m (except for one outlier higher

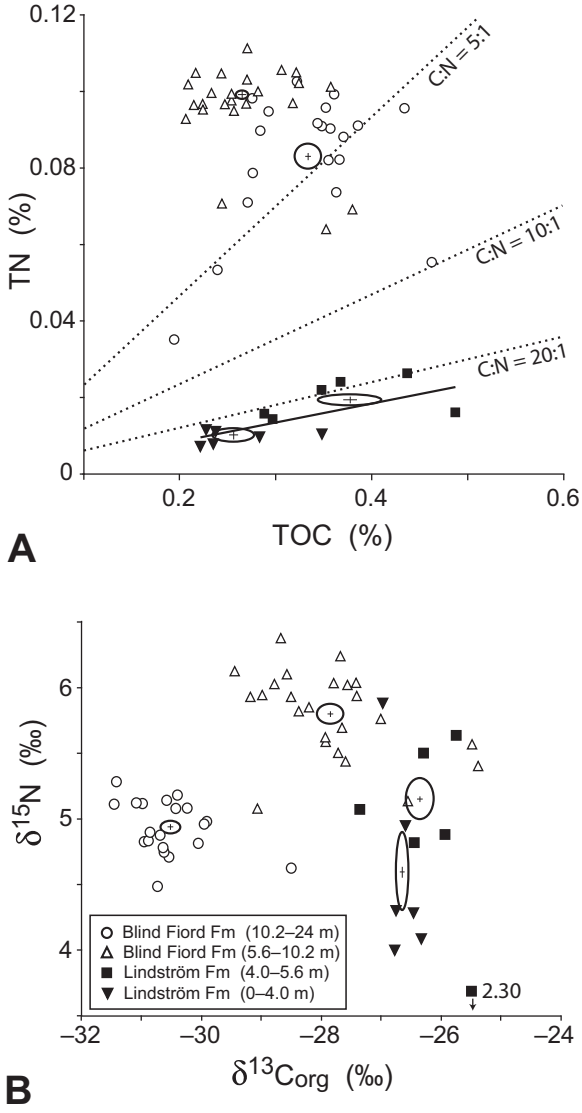

Figure 12. (A) TOC (total organic carbon) versus TN (total nitrogen) and (B) $\delta^{13}C_{org}$ versus $\delta^{15}N$. Crosses enclosed by ovals show the mean ± the standard error of the mean for each of four sample groups.

in the section), followed by a gradual decrease through the remainder of the section (Fig. 13C). Reactive Fe concentrations are nearly equivalent to total Fe in the Lindström Formation but decline to 50%–70% of total Fe values in the Blind Fiord Formation. Pyrite Fe covaries positively with total Fe but comprises no more than 25% of total Fe in the pyrite-rich intervals and <10% of total Fe in the pyrite-poor intervals.

The pyrite $\delta^{34}S$ profile, while varying over an ~40‰ range through much of the study section, exhibits marked changes in character in conjunction with event horizons (Fig. 13D). In the Lindström Formation, samples below datum A (4.0 m) show a systematic increase in $\delta^{34}S$ up section from –34‰ to –1‰. Above datum A, $\delta^{34}S_{py}$ values become highly variable, fluctuating between extremes of –40‰ and 0‰ from sample to sample. In the Blind Fiord Formation, a marked reduction in $\delta^{34}S_{py}$ variance is observed at the formation contact (5.6 m), such that $\delta^{34}S_{py}$ values are limited to the range of –40‰ to –28‰ in the 2 m of section just above the formation contact. Variance increases up section toward the latest Permian mass extinction horizon (10.2 m) but decreases again above the latest Permian mass extinction, where most samples yield $\delta^{34}S_{py}$ values between –40‰ and –30‰ (Fig. 13D).

The magnetic susceptibility signal in marine sediments is generally dominated by ferrimagnetic Fe-oxyhydroxides and paramagnetic clay minerals such as illite, i.e., minerals of detrital rather than authigenic origin (Ellwood et al., 2000, 2007). Magnetic susceptibility values in the Lindström Formation are about average for marine sedimentary rocks (<0.5 × 10^{-7} m^3 kg^{-1}) below datum A (4.0 m), but they exhibit a transient positive excursion (to ~1.0 × 10^{-7} m^3 kg^{-1}) between datum A and the formation contact (Fig. 13E). Magnetic susceptibility values in the Blind Fiord Formation rise sharply above the formation contact (5.6 m) to a maximum of ~3 × 10^{-7} m^3 kg^{-1} at 7.5 m and then decline gradually upward through the remainder of the section. There is little or no change in the magnetic susceptibility profile at the level of the latest Permian mass extinction horizon (10.2 m). Relationships between magnetic susceptibility and other proxies can assist in identifying the main carriers of the magnetic susceptibility signal. Magnetic susceptibility correlates most strongly with nonpyrite Fe (r = +0.89; $p[\alpha] < 0.001$; n = 56; Fig. 15A) and more weakly with clay minerals (r = +0.61; Fig. 15B) and other sediment fractions. This observation suggests that the magnetic susceptibility signal is carried primarily by detrital ferrimagnetic phases such as fine-grained Fe-oxyhydroxides, although clay minerals (mainly illite) may make a secondary contribution to the magnetic susceptibility signal (cf. Ellwood et al., 2007). Magnetic susceptibility also exhibits positive covariation with P concentrations (r = +0.60), possibly because of absorption of P onto Fe-oxyhydroxides (Föllmi, 1996).

DISCUSSION

Paleoredox Conditions and Environmental Changes

Paleoredox conditions in the West Blind Fiord study section can be inferred from a combination of petrographic, chemostratigraphic, and biomarker proxies. Although not entirely consistent, these proxies document a general change from less-reducing to more-reducing conditions upward within the section. Differences in redox interpretations among proxies may reflect differences in the time scales at which each proxy imparts its characteristic signature to the sediment. Such differences can result when redox conditions in the depositional system vary at time scales shorter than the depositional time represented by individual samples, which is ~1 k.y. for the Lindström Formation and ~0.1 k.y. for the Blind Fiord Formation (for 1- to 2-cm-thick samples; see Age model and sedimentation rates section; cf. Bond and Wignall, 2010). For example, if a largely oxic facies experiences short episodes of anoxia, it may not accumulate sufficient amounts of pyrite and redox-sensitive trace metals to document these events yet is likely to yield biomarkers with an anoxic signature, because even low concentrations of compounds such as aryl isoprenoids are taken as evidence of photic-zone euxinia (Summons and Powell, 1987; Grice et al., 2005; Cao et al., 2009). A similar phenomenon in which short intervals of oxygenation occur within an

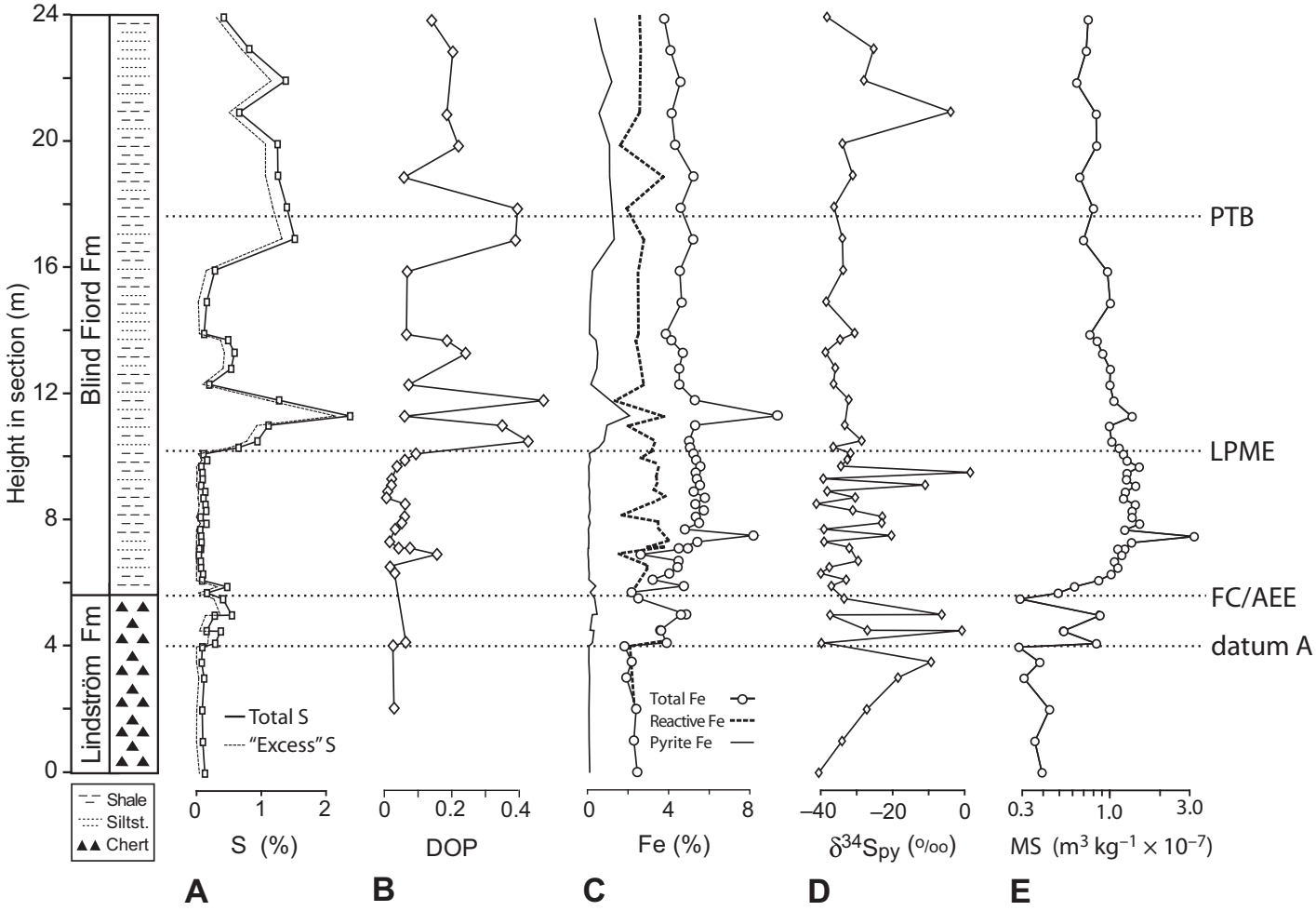

Figure 13. Chemostratigraphy (S-Fe system): (A) S, (B) degree of pyritization (DOP), (C) Fe, (D) pyrite $\delta^{34}S$, and (E) magnetic susceptibility (MS). In A, excess S represents the amount of pyrite S in excess of that expected for a given quantity of TOC in an ancient marine sediment deposited under oxic-suboxic conditions; it was calculated as S_{pyrite} – TOC/1.8 (Eq. 9 of Methods supplement [see text footnote 1]), where the coefficient 1.8 represents the average weight ratio of TOC to pyrite S in oxic-suboxic marine sediments (Raiswell and Berner, 1986). In C, pyrite Fe was calculated as S_{pyrite} × 55.85/64.12 (Eq. 10 of Methods supplement [see text footnote 1]), where the coefficients 55.85 and 64.12 represent the molar weights of Fe and S in stoichiometric pyrite, respectively. Abbreviations: AEE—Arctic extinction event; FC—formation contact; LPME—latest Permian mass extinction; PTB—Permian-Triassic boundary.

otherwise anoxic facies can result in juxtaposition of bioturbation with geochemical signatures of anoxia (Kenig et al., 2004).

The lower part of the Lindström Formation (0–4 m) was deposited under largely oxic conditions. This inference is based on low degree of pyritization values (<0.1; Fig. 13B) and U and Mo concentrations close to PAAS (Figs. 6E–6F). In addition, uniformly low S concentrations (<0.2%; Fig. 13A) and relatively ^{34}S-enriched pyrite S-isotopic values (Fig. 13D) provide no evidence for the presence of syngenetic pyrite (i.e., pyrite formed from H_2S-bearing waters) and, thus, of water-column euxinia. The upper part of the Lindström Formation (4.0–5.6 m) was deposited under conditions that were mainly suboxic, but ranged to weakly euxinic (i.e., marked by low H_2S concentrations). This inference is based on the observations that degree of pyritization values (<0.2; Fig. 13B) and U concentrations (mostly <4 ppm; Fig. 6E) remain low, but that Mo concentrations rise sharply above background detrital levels to ~8 ppm (Fig. 6F). S concentrations show a modest increase (to ~0.5%) associated mainly with excess S (Fig. 14) that may be present in the form of syngenetic framboidal pyrite (cf. Leventhal, 1983), an inference supported by a shift toward somewhat more ^{34}S-depleted pyrite sulfur (Fig. 13D; Lyons, 1997; Wilkin and Arthur, 2001). Finally, $\delta^{15}N$ values shift toward more ^{15}N-enriched compositions (Fig. 10C), consistent with enhanced denitrification under suboxic conditions (Jenkyns, 2010).

The lower part of the Blind Fiord Formation (5.6–10.2 m) was deposited under redox conditions similar to or somewhat more oxidizing than those of the underlying upper Lindström Formation. This interval exhibits low values for (1) DOP (<0.2; Fig. 13B), (2) redox-sensitive trace metals such as U and Mo (Figs. 6E–6F), and (3) excess S concentrations (Fig. 13A). However, pyrite sulfur compositions continue to show the ^{34}S-depleted values characteristic of syngenetic pyrite (Fig. 13D), and relatively high $\delta^{15}N$ values (Fig. 10C) are consistent with denitrification under suboxic conditions. Beginning at the latest Permian mass extinction horizon (10.2 m), redox proxies imply that the Blind Fiord Formation was deposited under more strongly reducing conditions. Degree of

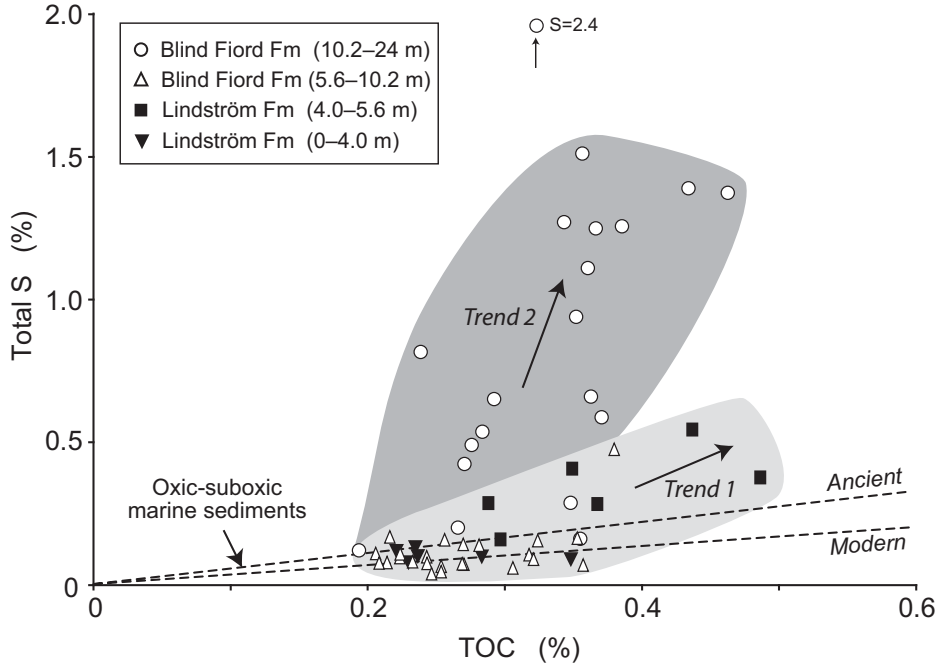

Figure 14. Total organic carbon (TOC) versus total S. Total S, which consists of >95% pyrite S, is plotted in preference to pyrite S owing to a greater number of analyses. Trends 1 and 2 reflect positive TOC-S covariation associated with intervals 4.0–5.6 m and 10.2–24 m, respectively, which contain excess S of probable syngenetic origin. For comparison, C-S trends for modern (C/S = 2.8; Berner and Raiswell, 1983) and ancient (C/S = 1.8; Raiswell and Berner, 1986) oxic-suboxic marine sediments are shown as dashed lines.

pyritization shows a sharp increase at the latest Permian mass extinction and generally higher values to the section top (Fig. 13B). Although the actual values (mostly 0.2–0.5) are not representative of euxinic conditions (cf. Raiswell et al., 1988; Lyons and Berner, 1992), we infer that euxinia was a transient phenomenon at West Blind Fiord that failed to yield the reactive Fe enrichments that typify persistently euxinic basins (Lyons and Severmann, 2006). It should be noted that elevated sedimentation rates, as developed at West Blind Fiord above the formation contact (see Age model and sedimentation rates section), can lead to lower-than-expected degree of pyritization values in euxinic facies, e.g., values of ~0.4 along the modern Black Sea margin (Lyons and Severmann, 2006). S increases locally to >2% above the latest Permian mass extinction horizon (Fig. 13A) and consists mainly of excess S that cannot be accounted for through degradation of sedimentary organic matter and, hence, is likely to represent syngenetic pyrite (Fig. 14). Values of $\delta^{34}S_{py}$ become more consistently negative (–30‰ to –40‰, with a single outlier; Fig. 13D), supporting the hypothesis that the pyrite fraction is composed largely of framboids formed in the water column rather than authigenic pyrite formed in the sediment (cf. Wilkin and Arthur, 2001; Nielsen and Shen, 2004; Algeo et al., 2008). Pyrite framboids were observed petrographically at a similar stratigraphic level at Buchanan Lake, a section located further toward the center of the Sverdrup Basin (Grasby and Beauchamp, 2009). These observations are consistent with an increase in the frequency and/or duration of water-column euxinia, although the relatively low degree of pyritization values and absence of U and Mo enrichment (Figs. 6E–6F) may indicate that euxinia continued to develop sporadically in a water mass of generally oxic or suboxic character.

Biomarker data provide some additional information about redox conditions in the West Blind Fiord section, although subject to certain caveats. Aryl isoprenoids (AI) with a 2,3,6-methyl substitution pattern are derived from the diagenetic breakdown of the carotenoid isorenieratene and chlorobactene, part of the light-harvesting complex of green sulfur bacteria (Chlorobiaceae), which are photosynthetic microorganisms that require hydrogen sulfide as an electron donor and, thus, are obligate anaerobes found only in environments with photic-zone euxinia (Summons and Powell, 1987; Overmann et al., 1992; Schouten et al., 2001; Brocks et al., 2005). In strongly reducing diagenetic environments, isorenieratene is reduced to isorenieratane. Increasing thermal maturation leads to progressive rupture of the isoprenoid chain, yielding a homologous series of monoaromatic compounds between C_{14} and C_{31} (Summons and Powell, 1987). AIs were identified in at least trace quantities in all samples from the West Blind Fiord section (Fig. 10D), but the quantities are smaller relative to TOC (<12 ng/g) compared to other Permian-Triassic boundary sections (Grice et al., 2005; Cao et al., 2009) and do not show any systematic stratigraphic trend. The AI profile is consistent with sporadic but transient development of euxinic conditions at West Blind Fiord throughout the study interval.

Of the biomarker proxies measured in the saturated hydrocarbon fraction, the ratio of 28,30-dinorhopane to C_{30} hopane (28,30-DNH ratio) and the homohopane index (HHI) have been used as indicators for water-column anoxia (Curiale and Odermatt, 1989; Peters et al., 2004). In the West Blind Fiord samples, the 28,30-DNH ratio increases from the Lindström Formation to the Blind Fiord Formation, but it is generally high in all the samples measured (Fig. 10E). Homohopanes, a series of C_{31}-C_{35} hopane hydrocarbons, are formed as breakdown products of bacteriohopanepolyols (Ourisson et al., 1979; Rohmer et al., 1984). The ratio of the C_{35}/C_{34} homohopanes (or HHI) records the preferential preservation of the C_{35} precursor hydrocarbon. Values >0.5 can be interpreted as evidence of anoxic conditions (Peters et al., 2004), although this proxy is also subject to a maturity influence. The homohopane index shows only modest variation through the study section, with values between 0.5 and 1.0, with the exception of a single outlier (2.7) just above the latest Permian mass extinction horizon at 10.2 m (Fig. 10H). Given the likely uniform thermal maturity of all samples in the study, these values suggest that reducing conditions prevailed throughout deposition of the West Blind Fiord section, with moderate intensification of anoxia in conjunction with the latest Permian mass extinction. The biomarker data are consistent with the hypothesis that photic-zone euxinia developed intermittently and for intervals of short duration at West Blind Fiord, although with an increase in the frequency and/or duration of such episodes following the global mass extinction event.

Plankton Community and Changes in Primary Productivity

Fossil and molecular evidence of major changes in the composition of phytoplankton communities can be observed in some stratigraphic sections following the latest Permian

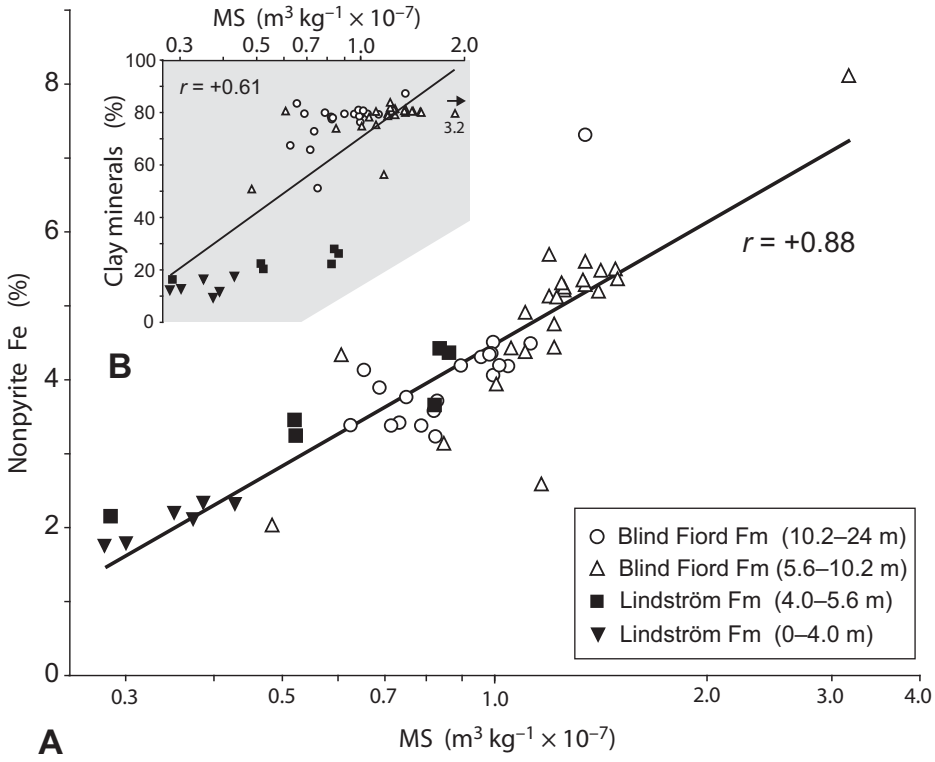

Figure 15. (A) Magnetic susceptibility (MS) versus nonpyrite Fe and (B) magnetic susceptibility versus clay minerals. In A, nonpyrite Fe was calculated as $Fe_{total} - Fe_{pyrite}$ (see Fig. 13C). Magnetic susceptibility exhibits strong positive covariation ($r = +0.89$; $p[\alpha] < 0.001$; $n = 56$) with nonpyrite-Fe concentration (Fig. 13C) but weaker covariation ($r = +0.61$) with clay-mineral abundance (Fig. 9A). These relationships suggest that the magnetic susceptibility signal is carried mainly by Fe-oxyhydroxides and secondarily by clay minerals such as illite.

mass extinction. In general, eukaryotic marine algae declined (Knoll et al., 2007; Chen et al., 2011), although prasinophyte and acritarch "disaster taxa" appear to have thrived (Payne and van de Schootbrugge, 2007). Photosynthetic prokaryotes, namely, green sulfur and N-fixing cyanobacteria, also thrived (Grice et al., 2005; Xie et al., 2005, 2007; Hays et al., 2007; Cao et al., 2009). Biomarker data from the West Blind Fiord study section suggest that changes in the phytoplankton community of the Sverdrup Basin during the latest Permian may have been relatively minor. First, aryl isoprenoids indicate the presence of green sulfur bacteria throughout the study interval, with a consistently high abundance just below the latest Permian mass extinction horizon (Fig. 10D). The short-term shifts toward higher $\delta^{13}C_{org}$ values at 7.5 m and 10.2 m (Fig. 10B) might be due to transient increases in biomass coming from Chlorobiaceae owing to the relatively ^{13}C-enriched composition of these bacteria (Riccardi et al., 2007). Second, the 2-MeHI profile documents a limited and relatively uniform presence of diazotrophic (N-fixing) cyanobacteria throughout the study section (Fig. 10G). Concentration increases at 1.0 m, 5.0 m, and 10.2 m suggest transient increases in cyanobacterial productivity (Summons et al., 1999; Xie et al., 2007). Each peak coincides with a shift toward lower $\delta^{15}N$ values (Fig. 10C), consistent with enhanced N fixation by diazotrophic cyanobacteria (Jenkyns et al., 2001; Kuypers et al., 2004). Third, shifts in the C_{27}/C_{29} sterane ratio (Fig. 10F) may reflect variability in the types of photosynthetic eukaryotes, specifically, red versus green algae, contributing organic matter to the sediments (Volkman et al., 1998; Peters et al., 2004). If correct, the increase in C_{27}/C_{29} sterane ratios at the formation contact at West Blind Fiord suggests enhanced proportions of red algae, which have a lower requirement for iron, making them better adapted to euxinic conditions than green algae. However, the ratios for this proxy are all close to 1.0, indicating that any changes in the proportions of the two groups of algae were modest at most. It can be observed that trends in the C_{27}/C_{29} sterane profile are opposite those in the 2-MeHI profile (Fig. 10G), suggesting that algal communities varied in tandem with abundances of diazotrophic cyanobacteria.

Evaluating changes in primary productivity in paleomarine systems is difficult, but qualitative inferences may be possible for the West Blind Fiord study section. C_{org}/N ratios of 20–30:1 in the Lindström Formation (Fig. 12A) may record comparatively high concentrations of terrestrial organic matter (Meyers, 1994), an inference supported by petrographic observations of higher-plant–derived organic macerals in samples close to the formation contact (Fig. 11). C_{org}/N ratios are mostly <5:1 in the Blind Fiord Formation (Fig. 12A), suggesting dominance of marine algal over terrestrial organic matter (Meyers, 1994). Although control of the shift in C_{org}/N ratios by changes in organic matter preservation related to more reducing conditions higher in the section cannot be excluded, several factors argue against such a mechanism: (1) The largest shift in C_{org}/N ratios is located at the formation contact (5.6 m), not at the latest Permian mass extinction (10.2 m), where the most pronounced intensification of reducing conditions occurred (see Paleoredox conditions and environmental changes section), and (2) the interval of the Blind Fiord Formation deposited under more oxidizing conditions (5.6–10.2 m) shows lower C_{org}/N ratios than the interval deposited under more reducing conditions (10.2–24 m; Fig. 12A). Thus, it seems likely that a large increase in the flux of marine algal material to the sediment occurred at the formation contact, probably in response to an increase in marine primary productivity.

Detrital Fluxes and Weathering Rate Changes

Major changes in subaerial weathering processes may have played an important role in the Permian-Triassic marine biotic crisis (Algeo et al., 2011). Globally, marine sections exhibit an average approximately sevenfold increase in sediment flux across the latest Permian mass extinction horizon (Algeo and Twitchett, 2010). Within the latest Permian interval of the West Blind Fiord study section, sedimentation rates increased by a factor of 3.5×, from 25 to 88 m m.y.$^{-1}$ (Fig. 4B), and even higher sediment fluxes characterize the Lower Triassic of the northern Pangean margin (Algeo and Twitchett, 2010, their fig. 2). However, even before the major increase in sediment flux that occurred at the formation contact (Fig. 9B), the composition of the detrital fraction at West Blind Fiord had begun to change: High field strength elements show a gradual shift from a rhyodacitic composition in the Lindström Formation to an average upper-crustal composition (PAAS) in the Blind Fiord Formation (Fig. 8). Although this pattern could be interpreted in terms of changing sediment

provenance (Dickinson, 1985), we infer that it reflects a gradual increase in subaerial weathering intensity. Secular changes in weathering intensity are supported by the CIA profile, which increases from 0.52–0.70 at 0–4.0 m to 0.80–0.85 at 4.0–5.6 m (Fig. 6G). The large increase in CIA values just below the formation contact (5.6 m) may represent a short-term erosional event, e.g., a rapid stripping of highly weathered soils from adjacent landmasses (cf. Sephton et al., 2005). The subsequent decline in CIA across the formation contact to intermediate values (~0.68–0.73) may reflect influx of less fully weathered material following the loss of terrestrial soils (cf. Algeo and Twitchett, 2010). This interpretation is supported by the magnetic susceptibility profile (Fig. 13E): The transient increase at 4.0–5.6 m is consistent with a major influx of soil-derived material (especially from the Fe-enriched B horizon), while the subsequent sustained increase above the formation contact (5.6 m) reflects an elevated flux of Fe-bearing clay minerals produced through intensified chemical weathering. Intensified soil erosion and chemical weathering around the latest Permian mass extinction have been inferred in earlier studies of both terrestrial (Retallack, 2005; Sheldon, 2006) and marine sections (Sephton et al., 2005; Xie et al., 2007; Wang and Visscher, 2007).

Relationship to Early Eruptions of Siberian Traps?

The Siberian Traps flood basalt eruptions are thought to have caused major global environmental changes. Release of a combination of volcanic CO_2 and volcanogenic methane produced when magma intruded Siberian coal basins triggered strong climatic warming (Retallack, 1999), as shown by oxygen isotope studies (Korte et al., 2005a, 2005b; Kearsey et al., 2009). Higher levels of atmospheric CO_2 along with volcanic SO_2 emissions are likely to have increased the acidity of precipitation (Wignall, 2001, 2007), which, in combination with warmer temperatures, resulted in elevated rates of chemical weathering (Retallack, 1999; Sheldon, 2006). These changes may have been important factors in the latest Permian destruction of terrestrial ecosystems, when gymnosperm-dominated forests representing a mature successional stage yielded to rapidly growing lycopsid-fern communities representing an early successional stage (Wang, 1996; Looy et al., 2001; Grauvogel-Stamm and Ash, 2005; Hochuli et al., 2010; Hermann et al., 2011). The destruction of terrestrial vegetation had profound consequences for weathering processes, nutrient fluxes, and marine environmental conditions. A combination of climate warming and increased nutrient fluxes (eutrophication) resulted in greatly expanded oceanic anoxia (Winguth and Maier-Reimer, 2005; Meyer et al., 2008; Algeo et al., 2010). Shallow-marine ecosystems were harmed by episodic expansion of the oxygen-minimum zone into the ocean-surface layer as well as by elevated particulate fluxes (siltation) in paralic environments. High rates of terrestrial erosion persisted widely for up to ~2 m.y. during the Early Triassic and were potentially a factor in the delayed recovery of marine biotas (Algeo and Twitchett, 2010; Algeo et al., 2011), although stable refugia are known to have existed (Beatty et al., 2008).

We propose that changes in the marine environment and biota of the Sverdrup Basin during the Late Permian were driven by perturbations to adjacent land areas in response to Siberian Traps volcanism (Fig. 16). Silicic eruptions and magmatic intrusions into Siberian coalfields are

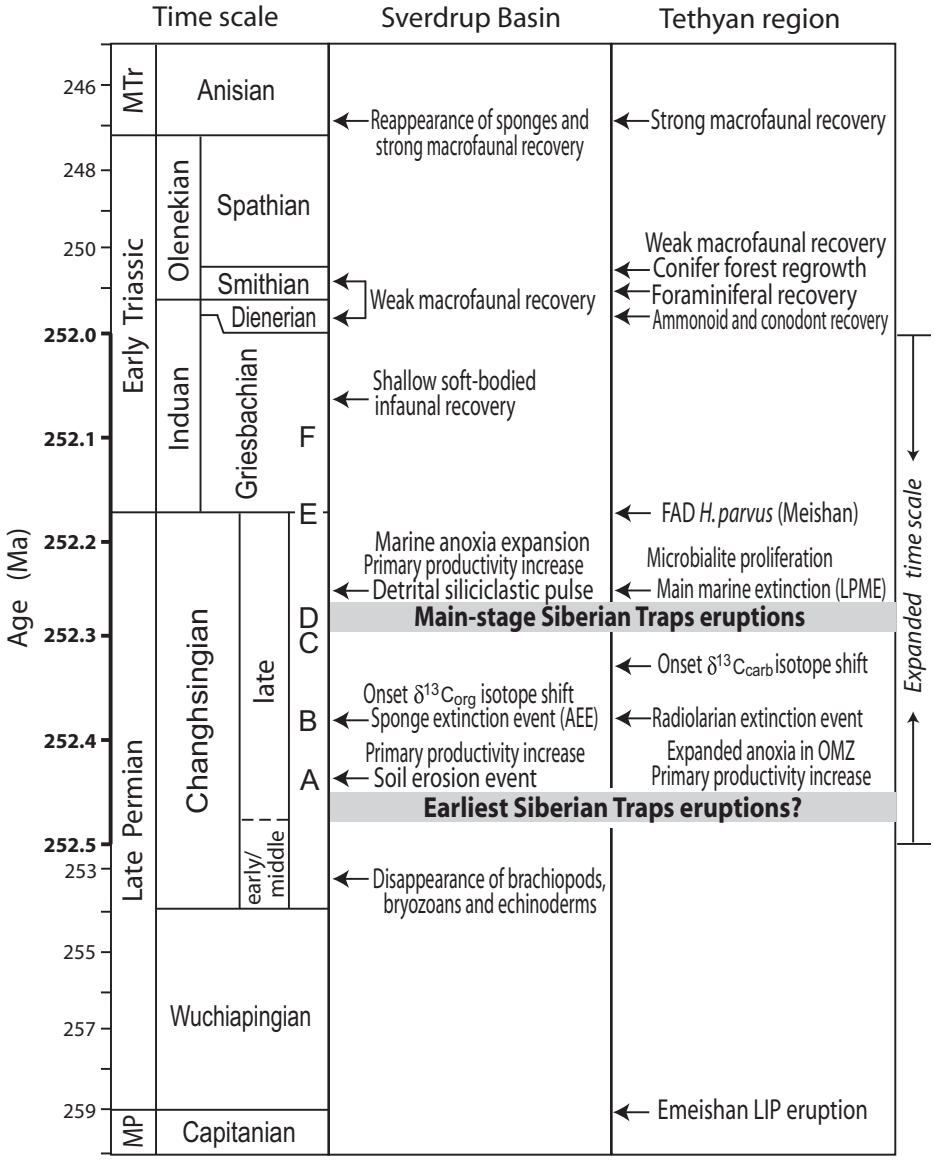

Figure 16. Time line of events in the Sverdrup Basin and Tethyan region during the Late Permian and Early Triassic. Late Changhsingian extinctions of sponges in the Sverdrup Basin and radiolarians in the Tethyan region predate main-stage Siberian Traps eruptions by ~100 k.y. and may have been associated with early stage explosive silicic eruptions (cf. Grasby et al., 2011). Note expanded time scale between 252.5 and 252.0 Ma. A to F refer to correlation datums in Figures 4A and 5. MP—Middle Permian, MTr—Middle Triassic; LPME—latest Permian mass extinction; AEE—Arctic extinction event; FAD—first appearance datum; OMZ—oxygen minimum zone; LIP—large igneous province.

likely to have resulted in deposition of toxic gases and ash that degraded or destroyed terrestrial floras (Grasby et al., 2011; cf. Self et al., 2008), leading to large-scale erosion of soils with consequent detrimental effects on marine ecosystems (Algeo et al., 2011). Pre–main-stage eruptions are thought to have begun during the early late Changhsingian (Kozur and Weems, 2011; Grasby et al., 2011), up to several hundred thousand years prior to the latest Permian mass extinction and thus roughly contemporaneous with marine environmental changes in the Sverdrup Basin (this study) and with changes in intermediate-depth marine systems globally (see Introduction section). In the following, we summarize the pattern of marine environmental changes discussed above in reference to the main event horizons at West Blind Fiord.

Datum A (4.0 m) in the upper Lindström Formation is the first horizon recording major environmental changes within the study section. At this level, the detrital fraction underwent a compositional change toward higher Fe-oxyhydroxide concentrations and a CIA signature indicative of greater weathering intensity. High CIA values may be an indication of a large particulate contribution from soils, where strong cation leaching is common (Maynard, 1992), and the pulse of Fe-oxyhydroxides may reflect erosion of the Fe-rich B horizons of soils. This event was accompanied by a modest shift toward more reducing conditions, probably caused by elevated fluxes of soil-derived nutrients that triggered an increase in marine productivity. Concurrently, the abundance of siliceous sponges, the most prominent remaining component of the Late Permian biota in the Sverdrup Basin, was reduced modestly, probably in response to changing nutrient and/or redox conditions.

The formation contact (5.6 m) between the Lindström and Blind Fiord formations records the final extinction of siliceous sponges in the Sverdrup Basin, herein termed the "Arctic extinction event." A concurrent large increase in detrital sediment flux may have been the primary cause of this event. A shift toward lower C_{org}:N ratios is indicative of a larger fraction of marine organic matter, and higher C_{27}/C_{29} ratios may reflect greater abundance of algal- or bacterial-consuming ciliated protozoans. Both patterns are consistent with an increase in marine productivity, which is a likely consequence of enhanced terrestrial inputs to marine systems (Algeo et al., 2011). A shift toward less-reducing conditions across the formation contact may have been related to enhanced freshwater runoff into the Sverdrup Basin in conjunction with higher detrital sediment fluxes.

The latest Permian mass extinction (10.2 m) is not characterized by any apparent change in the fossil biota (since all macrofauna had disappeared earlier) or marine productivity, nor did it have any noticeable effect on the composition of the detrital fraction or subaerial weathering intensity. The most significant changes at this level are related to benthic redox conditions, which became more persistently and/or more intensely euxinic, as recorded by multiple redox proxies, although changes in phytoplankton community composition may have occurred at the same time, as proxied by $\delta^{13}C_{org}$ and $\delta^{15}N$. Persistently euxinic conditions reflect a sustained shallowing of the Sverdrup Basin chemocline to the water depth of the West Blind Fiord study site. One possibility is that chemocline shallowing was driven by enhanced marine productivity, which had accelerated at the formation contact (~100 k.y. earlier) and may have coincidentally peaked at the latest Permian mass extinction. An alternative is that the chemocline shallowed abruptly at the latest Permian mass extinction due to global climatic warming triggered by release of volcanic CO_2 or coalfield methane (Retallack, 1999), resulting in a rapid reduction of the solubility of dissolved oxygen in seawater (but see Bond and Wignall [2010] for an opposing view). The latter process could have been triggered by the onset of the main stage of Siberian Traps volcanism (Reichow et al., 2009).

An important issue is the apparent difference in timing of terrestrial disturbances in the Boreal and Tethyan regions. An increased flux of detrital siliciclastics to the Sverdrup Basin commenced in the early part of the late Changhsingian (this study), whereas the Tethyan region did not experience this influx until the latest Changhsingian, just prior to the latest Permian mass extinction (Sephton et al., 2005; Xie et al., 2005, 2007; Algeo et al., 2007; Wang and Visscher, 2007). We suggest that the key difference was paleolatitude. More northerly sites may have been more vulnerable to deposition of acidic gases and ash from early stages of the Siberian Traps eruptions (Fig. 16; Grasby et al., 2011; cf. Self et al., 2008). In the latest Permian, the West Blind Fiord study site was located at ~40°N, which was much closer to the Siberian Traps volcanic centers at 60–70°N in terms of both paleolatitude and absolute distance (~3000–4000 km) than sites in the Tethyan region (Fig. 1, inset). Following explosive silicic eruptions, fallout is commonly initially constrained to a narrow latitudinal belt, and the intensity of fallout diminishes considerably as it spreads to higher and lower latitudes (cf. McCormick et al., 1995; Robock, 2002). The environmental effects of volcanic emissions can be regionally and/or latitudinally constrained, as following the 1783 Laki eruption in Iceland (Thordarson and Self, 2003). Sulfate emissions, in particular, can have environmentally harmful effects related to acidification of soils and surface waters and metabolic toxicity (Thordarson and Self, 2003; Ward, 2009; Bao et al., 2010). Such effects may have been "felt" in the boreal Sverdrup Basin sooner than in the peri-equatorial Tethyan region.

CONCLUSIONS

The West Blind Fiord section on southwestern Ellesmere Island provides a record of deteriorating environmental conditions in the Sverdrup Basin during the late Changhsingian (late Late Permian). Environmental deterioration proceeded stepwise, with most change associated with a few stratigraphic horizons. Datum A, of early late Changhsingian age, records increased Fe-oxyhydroxide fluxes and weathering intensity as well as modest shifts toward more-reducing water-mass conditions and higher marine productivity, recording an initial disturbance that washed soils into the marine environment. The contact between the Lindström Formation and the overlying Blind Fiord Formation, ~50 k.y. younger than datum A, records a large increase in detrital sediment flux, elevated marine productivity, and the disappearance of siliceous sponges during the Arctic extinction event. The horizon equivalent to the global latest Permian mass extinction, ~100 k.y. younger than the Arctic extinction event, records strong intensification of anoxia and possible changes in phytoplankton community composition. Compared to some sections, Meishan in particular, the phytoplankton community remained relatively stable throughout the study interval, although characterized by recurrent increases in the relative abundances of green sulfur bacteria and diazotrophic cyanobacteria and, perhaps, an increase in the ratio of red to green algae above the Arctic extinction event. These patterns are consistent with a fluctuating but generally rising chemocline in the Sverdrup Basin during the latest Permian, probably triggered by an increase in seawater nutrient levels and, at the latest Permian mass extinction, a reduction in dissolved oxygen solubility due to climatic warming. These changes in the marine environment were ultimately driven by increasing detrital sediment fluxes resulting from terrestrial ecosystem degradation, possibly related to early stage explosive silicic eruptions of Siberian Traps volcanic centers. The deleterious effects of these eruptions may have been felt sooner in the Boreal region than in the peri-equatorial Tethyan region owing to latitudinally concentrated fallout of toxic gas and ash.

ACKNOWLEDGMENTS

We thank Tim Phillips for drafting services, Tammie Gerke and Warren Huff for analytical assistance, Matthew Clapham and Richard Twitchett for reviews of the manuscript, and Brian Pratt for editorial handling. We gratefully acknowledge support from the National Science Foundation to Algeo (EAR-0618003, EAR-0745574, and EAR-1053449), from the Canadian Natural Sciences and Engineering Research Council to Henderson, and from the National Aeronautics and Space Administration Exobiology Program to Summons and Hays. This paper is a contribution to International Geological Correlation Programme Project 572.

REFERENCES CITED

Algeo, T.J., and Twitchett, R.J., 2010, Anomalous Early Triassic sediment fluxes due to elevated weathering rates and their biological consequences: Geology, v. 38, p. 1023–1026, doi:10.1130/G31203.1.

Algeo, T.J., Ellwood, B.B., Nguyen, T.K.T., Rowe, H., and Maynard, J.B., 2007, The Permian-Triassic boundary at Nhi Tao, Vietnam: Evidence for recurrent influx of sulfidic watermasses to a shallow-marine carbonate platform: Palaeogeography, Palaeoclimatology, Palaeoecology, v. 252, p. 304–327, doi:10.1016/j.palaeo.2006.11.055.

Algeo, T.J., Shen, Y., Zhang, T., Lyons, T.W., Bates, S.M., Rowe, H., and Nguyen, T.K.T., 2008, Association of ^{34}S-depleted pyrite layers with negative carbonate $\delta^{13}C$ excursions at the Permian/Triassic boundary: Evidence for upwelling of sulfidic deep-ocean watermasses: Geochemistry, Geophysics, Geosystems, v. 9, Q04025, 10 p.

Algeo, T.J., Hinnov, L., Moser, J., Maynard, J.B., Elswick, E., Kuwahara, K., and Sano, H., 2010, Changes in productivity and redox conditions in the Panthalassic Ocean during the latest Permian: Geology, v. 38, p. 187–190, doi:10.1130/G30483.1.

Algeo, T.J., Chen, Z.Q., Fraiser, M.L., and Twitchett, R.J., 2011, Terrestrial-marine teleconnections in the collapse and rebuilding of Early Triassic marine ecosystems: Palaeogeography, Palaeoclimatology, Palaeoecology, v. 308, p. 1–11, doi:10.1016/j.palaeo.2011.01.011.

Allen, P.A., and Allen, J.R., 2005, Basin Analysis: Principles and Applications (2nd ed.): Oxford, UK, Blackwell, 560 p.

Alroy, J., and 34 others, 2008, Phanerozoic trends in the global diversity of marine invertebrates: Science, v. 321, p. 97–100, doi:10.1126/science.1156963.

Bao, H., Yu, S., and Tong, D.Q., 2010, Massive volcanic SO_2 oxidation and sulphate aerosol deposition in Cenozoic North America: Nature, v. 465, p. 909–912, doi:10.1038/nature09100.

Baud, A., Nakrem, H.A., Beauchamp, B., Beatty, T.W., Embry, A.F., and Henderson, C.M., 2008, Lower Triassic bryozoan beds from Ellesmere Island, High Arctic, Canada: Polar Research, v. 27, p. 428–440, doi:10.1111/j.1751-8369.2008.00071.x.

Beatty, T.W., Zonneveld, J.-P., and Henderson, C.M., 2008, Anomalously diverse Early Triassic ichnofossil assemblages in northwest Pangea: A case for a shallow-marine habitable zone: Geology, v. 36, p. 771–774, doi:10.1130/G24952A.1.

Beauchamp, B., 1989, Lower Permian (Artinskian) sponge-bryozoan buildups, southwestern Ellesmere Island, Canadian Arctic Archipelago, *in* Geldsetzer, H.H.J., James, N.P., and Tebbutt, G.E., eds., Reefs, Canada and Adjacent Areas: Canadian Society of Petroleum Geologists Memoir 13, p. 575–584.

Beauchamp, B., 1994, Permian climatic cooling in the Canadian Arctic, *in* Klein, G.D., ed., Pangea: Paleoclimate, Tectonics and Sedimentation during Accretion, Zenith and Break-Up of a Super-Continent: Geological Society of America Special Paper 288, p. 229–246.

Beauchamp, B., and Baud, A., 2002, Growth and demise of Permian biogenic chert along northwest Pangea: Evidence for end-Permian collapse of thermohaline circulation: Palaeogeography, Palaeoclimatology, Palaeoecology, v. 184, p. 37–63, doi:10.1016/S0031-0182(02)00245-6.

Beauchamp, B., and Desrochers, A., 1997, Permian warm- to very cold carbonates and cherts in northwest Pangea, *in* James, N.P., and Clarke, J., eds., Cool Water Carbonates: Society of Economic Geologists and Paleontologists Special Publication 56, p. 327–347.

Beauchamp, B., and Henderson, C.M., 1994, The Lower Permian (Artinskian) Raanes, Great Bear Cape, and Trappers Cove formations, Sverdrup Basin, Canadian Arctic: Stratigraphy and conodont zonation: Bulletin of Canadian Petroleum Geology, v. 42, p. 565–600.

Beauchamp, B., Oldershaw, A.E., and Krouse, H.R., 1987, Upper Carboniferous to Upper Permian ^{13}C-enriched primary carbonates in the Sverdrup Basin, Canadian Arctic: Comparisons to coeval western North American ocean margins: Chemical Geology, v. 65, p. 391–413.

Beauchamp, B., Harrison, J.C., and Henderson, C.M., 1989a, Upper Paleozoic stratigraphy and basin analysis of the Sverdrup Basin, Canadian Arctic Archipelago: Part 1—Time frame and tectonic evolution, *in* Current Research Part G: Geological Survey of Canada Paper 89–1G, p. 105–113.

Beauchamp, B., Harrison, J.C., and Henderson, C.M., 1989b, Upper Paleozoic stratigraphy and basin analysis of the Sverdrup Basin, Canadian Arctic Archipelago: Part 2—Transgressive-regressive sequences, *in* Current Research Part G: Geological Survey of Canada Paper 89–1G, p. 115–124.

Beauchamp, B., Henderson, C.M., Grasby, S.E., Gates, L.T., Beatty, T.W., Utting, J., and James, N.P., 2009, Late Permian sedimentation in the Sverdrup Basin, Canadian Arctic: The Lindström and Black Stripe Formations: Bulletin of Canadian Petroleum Geology, v. 57, p. 167–191, doi:10.2113/gscpgbull.57.2.167.

Bensing, J.P., James, N.P., and Beauchamp, B., 2008, Carbonate deposition during a time of mid-latitude ocean cooling: Early Permian "subtropical" sedimentation in the Sverdrup Basin, Arctic Canada: Journal of Sedimentary Research, v. 78, p. 2–15, doi:10.2110/jsr.2008.004.

Benton, M.J., and Twitchett, R.J., 2003, How to kill (almost) all life: The end-Permian extinction event: Trends in Ecology & Evolution, v. 18, p. 358–365, doi:10.1016/S0169-5347(03)00093-4.

Berner, R.A., and Raiswell, R., 1983, Burial of organic carbon and pyrite sulfur in sediments over Phanerozoic time: A new theory: Geochimica et Cosmochimica Acta, v. 47, p. 855–862, doi:10.1016/0016-7037(83)90151-5.

Bond, D.P.G., and Wignall, P.B., 2010, Pyrite framboid study of marine Permian-Triassic boundary sections: A complex anoxic event and its relationship to contemporaneous mass extinction: Geological Society of America Bulletin, v. 122, p. 1265–1279, doi:10.1130/B30042.1.

Bowring, S.A., Erwin, D.H., Jin, Y.G., Martin, M.W., Davidek, K., and Wang, W., 1998, U/Pb zircon geochronology and tempo of the end-Permian mass extinction: Science, v. 280, p. 1039–1045, doi:10.1126/science.280.5366.1039.

Brocks, J.J., Love, G.D., Summons, R.E., Knoll, A.H., Logan, G.A., and Bowden, S.A., 2005, Biomarker evidence for green and purple sulphur bacteria in a stratified Palaeoproterozoic sea: Nature, v. 437, p. 866–870, doi:10.1038/nature04068.

Campbell, I.H., Czamanske, G.K., Fedorenko, V.A., Hill, R.I., and Stepanov, V., 1992, Synchronism of the Siberian Traps and the Permian-Triassic boundary: Science, v. 258, p. 1760–1763, doi:10.1126/science.258.5089.1760.

Cao, C., Wang, W., and Jin, Y., 2002, Carbon isotope excursions across the Permian-Triassic boundary in the Meishan section, Zhejiang Province, China: Kexue Tongbao (Chinese Science Bulletin), v. 47, p. 1125–1129, doi:10.1360/02tb9252.

Cao, C., Hays, L.E., Love, G.D., Bowring, S.A., Wang, W., Shen, S., and Summons, R.E., 2009, Biogeochemical evidence for euxinic oceans and ecological disturbance presaging the end-Permian mass extinction event: Earth and Planetary Science Letters, v. 281, p. 188–201, doi:10.1016/j.epsl.2009.02.012.

Catuneanu, O., and 27 others, 2009, Towards the standardization of sequence stratigraphy: Earth-Science Reviews, v. 92, p. 1–33, doi:10.1016/j.earscirev.2008.10.003.

Chen, J., Beatty, T.W., Henderson, C.M., and Rowe, H., 2009, Conodont biostratigraphy across the Permian-Triassic boundary at the Dawen section, Great Bank of Guizhou, Guizhou Province, South China: Implications for the Late Permian extinction and correlation with Meishan: Journal of Asian Earth Sciences, v. 36, p. 442–458, doi:10.1016/j.jseaes.2008.08.002.

Chen, L., Wang, Y., Xie, S., Kershaw, S., Dong, M., Yang, H., Liu, H., and Algeo, T.J., 2011, Molecular records of microbialites following the end-Permian mass extinction in Chongyang, Hubei Province, South China: Palaeogeography, Palaeoclimatology, Palaeoecology, v. 308, p. 151–159, doi:10.1016/j.palaeo.2010.09.010.

Chen, Z.Q., Tong, J., Liao, Z.T., and Chen, J., 2010, Structural changes of marine communities over the Permian-Triassic transition: Ecologically assessing the end-Permian mass extinction and its aftermath: Global and Planetary Change, v. 73, p. 123–140, doi:10.1016/j.gloplacha.2010.03.011.

Clark, D.L., 1959, Conodonts from the Triassic of Nevada and Utah: Journal of Paleontology, v. 33, no. 2, p. 305–312.

Curiale, J.A., and Odermatt, J.R., 1989, Short-term biomarker variability in the Monterey Formation, Santa Maria Basin: Organic Geochemistry, v. 14, p. 1–13, doi:10.1016/0146-6380(89)90014-4.

Dewing, K., Obermajer, M., and Goodarzi, F., 2007, Geological and Geochemical Data from the Canadian Arctic Islands: Part III. Organic Matter Reflectance Data: Geological Survey of Canada Open-File 5476, CD-ROM.

Dickinson, W.R., 1985, Interpreting provenance relations from detrital modes of sandstones, *in* Zuffa, G.G., ed., Provenance of Arenites: Dordrecht, Netherlands, D. Reidel, p. 333–361.

Ellwood, B.B., Crick, R.E., El Hassani, A., Benoist, S.L., and Young, R.H., 2000, Magnetosusceptibility event and cyclostratigraphy method applied to marine rocks: Detrital input versus carbonate productivity: Geology, v. 28, p. 1135–1138, doi:10.1130/0091-7613(2000)28<1135:MEACMA>2.0.CO;2.

Ellwood, B.B., Brett, C.E., and MacDonald, W.D., 2007, Magnetosusceptibility stratigraphy of the Upper Ordovician Kope Formation, northern Kentucky: Palaeogeography, Palaeoclimatology, Palaeoecology, v. 243, p. 42–54, doi:10.1016/j.palaeo.2006.07.003.

Embry, A.F., 1991, Mesozoic history of the Arctic Islands, *in* Trettin, H.P., ed., Geology of the Innuitian Orogen and Arctic Platform of Canada and Greenland: Geological Survey of Canada, Geology of Canada, no. 3 (also Geological Society of America, The Geology of North America, v. E), p. 369–433.

Embry, A.F., 2009, Crockerland—The source area for the Triassic to Middle Jurassic strata of northern Axel Heiberg Island, Canadian Arctic Islands: Bulletin of Canadian Petroleum Geology, v. 57, p. 129–140, doi:10.2113/gscpgbull.57.2.129.

Embry, A.F., and Beauchamp, B., 2008, Sverdrup Basin, Chapter 13, *in* Hsü, K.J., ed., Sedimentary Basins of the World, Volume 5: The Sedimentary Basins of the United States and Canada: Amsterdam, Netherlands, Elsevier, p. 451–471.

Erwin, D.H., 1994, The Permo-Triassic extinction: Nature, v. 367, p. 231–236, doi:10.1038/367231a0.

Feng, Q., He, W., Gu, S., Meng, Y., Jin, Y., and Zhang, F., 2007, Radiolarian evolution during the latest Permian in South China: Global and Planetary Change, v. 55, p. 177–192, doi:10.1016/j.gloplacha.2006.06.012.

Föllmi, K.B., 1996, The phosphorus cycle, phosphogenesis and marine phosphate-rich deposits: Earth-Science Reviews, v. 40, p. 55–124, doi:10.1016/0012-8252(95)00049-6.

Fralick, P., 2003, Geochemistry of clastic sedimentary rocks: Ratio techniques, *in* Lentz, D.R., ed., Geochemistry of Sediments and Sedimentary Rocks: Evolutionary Considerations to Mineral Deposit-Forming Environments: Geological Association of Canada, Geotext 4: St. John's, Newfoundland, Canada, p. 85–103.

Gates, L.M., James, N.P., and Beauchamp, B., 2004, A glass ramp: Shallow-water Permian spiculitic chert sedi-

mentation, Sverdrup Basin, Arctic Canada: Sedimentary Geology, v. 168, p. 125–147, doi:10.1016/j.sedgeo.2004.03.008.

Grasby, S.E., and Beauchamp, B., 2008, Chemostratigraphic record of the end-Permian extinction is a function of basin position: Chemical Geology, v. 253, p. 141–150, doi:10.1016/j.chemgeo.2008.05.005.

Grasby, S.E., and Beauchamp, B., 2009, Latest Permian to Early Triassic basin-to-shelf anoxia in the Sverdrup Basin, Arctic Canada: Chemical Geology, v. 264, p. 232–246, doi:10.1016/j.chemgeo.2009.03.009.

Grasby, S.E., Sanei, H., and Beauchamp, B., 2011, Catastrophic dispersion of coal fly ash into oceans during the latest Permian extinction: Nature Geoscience, v. 4, p. 104–107, doi:10.1038/ngeo1069.

Grauvogel-Stamm, L., and Ash, S.R., 2005, Recovery of the Triassic land flora from the end-Permian life crisis: Comptes Rendus, Palévol, v. 4, p. 593–608, doi:10.1016/j.crpv.2005.07.002.

Grice, K., Cao, C., Love, G.D., Böttcher, M.E., Twitchett, R.J., Grosjean, E., Summons, R.E., Turgeon, S.C., Dunning, W., and Jin, Y., 2005, Photic zone euxinia during the Permian-Triassic superanoxic event: Science, v. 307, p. 706–709, doi:10.1126/science.1104323.

Gröcke, D.R., Hesselbo, S., and Jenkyns, H.C., 1999, Carbon-isotope composition of Lower Cretaceous fossil wood: Ocean-atmosphere chemistry and relation to sea-level change: Geology, v. 27, p. 155–158, doi:10.1130/0091-7613(1999)027<0155:CICOLC>2.3.CO;2.

Grossman, E.L., Yancey, T.E., Jones, T.E., Bruckschen, P., Chuvashov, B., Mazzullo, S.J., and Mii, H.-S., 2008, Glaciation, aridification, and carbon sequestration in the Permo-Carboniferous: The isotope record from low latitudes: Palaeogeography, Palaeoclimatology, Palaeoecology, v. 268, p. 222–233, doi:10.1016/j.palaeo.2008.03.053.

Hallam, A., and Wignall, P.B., 1999, Mass extinctions and sea-level changes: Earth-Science Reviews, v. 48, p. 217–250, doi:10.1016/S0012-8252(99)00055-0.

Hays, L.E., Beatty, T., Henderson, C.M., Love, G.D., and Summons, R.E., 2007, Evidence for photic zone euxinia through the end-Permian mass extinction in the Panthalassic Ocean (Peace River Basin, western Canada): Palaeoworld, v. 16, p. 39–50, doi:10.1016/j.palwor.2007.05.008.

He, W.H., Shen, S.Z., Feng, Q.L., and Gu, S.Z., 2005, A late Changhsingian (Late Permian) deepwater brachiopod fauna from the Talung Formation at the Dongpan section, southern Guangxi, South China: Journal of Paleontology, v. 79, p. 927–938, doi:10.1666/0022-3360(2005)079[0927:ALCLPD]2.0.CO;2.

He, W.H., Shi, G.R., Feng, Q.L., Campi, M.J., Gu, S.Z., Bu, J.J., Peng, Y.Q., and Meng, Y.Y., 2007, Brachiopod miniaturization and its possible causes during the Permian-Triassic crisis in deep water environments, South China: Palaeogeography, Palaeoclimatology, Palaeoecology, v. 252, p. 145–163, doi:10.1016/j.palaeo.2006.11.040.

Heimhofer, U., Hochuli, P.A., Burla, S., Andersen, N., and Weissert, H., 2003, Terrestrial carbon-isotope records from coastal deposits (Algarve, Portugal): A tool for chemostratigraphic correlation on an intrabasinal and global scale: Terra Nova, v. 15, p. 8–13, doi:10.1046/j.1365-3121.2003.00447.x.

Henderson, C.M., 1993, Are Permian-Triassic boundary events diachronous? Evidence from the Canadian Arctic, *in* Annual Convention of Canadian Society of Petroleum Geologists with Global Sedimentary Geology Program—Carboniferous to Jurassic Pangea, Program and Abstracts: Calgary, Alberta, Canada, Canadian Society of Petroleum Geologists, p. 136.

Henderson, C.M., 1997, Uppermost Permian conodonts and the Permian-Triassic boundary in the Western Canada sedimentary basin: Bulletin of Canadian Petroleum Geology, v. 45, p. 693–707.

Henderson, C.M., and Baud, A., 1997, Correlation of the Permian-Triassic boundary in Arctic Canada and comparison with Meishan, China, *in* Proceedings of the 30th International Geological Congress, Volume 11: Utrecht, Netherlands, VSP Scientific Publishers, p. 143–152.

Henderson, C.M., and Mei, S., 2007, Geographical clines in Permian and Lower Triassic gondolellids and its role in taxonomy: Palaeoworld, v. 16, p. 190–201, doi:10.1016/j.palwor.2007.05.014.

Hermann, E., Hochuli, P.A., Bucher, H., Vigran, J.O., Weissert, H., and Bernasconi, S.M., 2010, A close-up view of the Permian-Triassic boundary based on expanded organic carbon isotope records from Norway (Trøndelag and Finnmark Platform): Global and Planetary Change, v. 74, p. 156–167, doi:10.1016/j.gloplacha.2010.10.007.

Hermann, E., Hochuli, P.A., Bucher, H., Brühwiler, T., Hautmann, M., Ware, D., and Roohi, G., 2011, Terrestrial ecosystems on North Gondwana following the end-Permian mass extinction: Gondwana Research, v. 20, p. 630–637, doi:10.1016/j.gr.2011.01.008.

Hochuli, P.A., Vigran, J.O., Hermann, E., and Bucher, H., 2010, Multiple climatic changes around the Permian-Triassic boundary event revealed by an expanded palynological record from mid-Norway: Geological Society of America Bulletin, v. 122, p. 884–896, doi:10.1130/B26551.1.

Isozaki, Y., Shimizu, N., Yao, J., Ji, Z., and Matsuda, T., 2007a, End-Permian extinction and volcanism-induced environmental stress: Permian-Triassic boundary interval of a lower-slope facies at Chaotian, South China: Palaeogeography, Palaeoclimatology, Palaeoecology, v. 252, p. 218–238, doi:10.1016/j.palaeo.2006.11.051.

Isozaki, Y., Kawahata, H., and Ota, A., 2007b, A unique carbon isotope record across the Guadalupian-Lopingian (Middle-Upper Permian) boundary in mid-oceanic paleo-atoll carbonates: The high-productivity "Kamura event" and its collapse in Panthalassa: Global and Planetary Change, v. 55, p. 21–38, doi:10.1016/j.gloplacha.2006.06.006.

Jenkyns, H.C., 2010, Geochemistry of oceanic anoxic events: Geochemistry, Geophysics, Geosystems, v. 11, no. 3, Q03004, 30 p.

Jenkyns, H.C., Gröcke, D.R., and Hesselbo, S.P., 2001, Nitrogen isotope evidence for water mass denitrification during the early Toarcian (Jurassic) oceanic anoxic event: Paleoceanography, v. 16, p. 593–603, doi:10.1029/2000PA000558.

Jiang, H., Lai, X., Luo, G., Aldridge, R., Zhang, K., and Wignall, P., 2007, Restudy of conodont zonation and evolution across the P/T boundary at Meishan section, Changxing, Zhejiang, China: Global and Planetary Change, v. 55, p. 39–55, doi:10.1016/j.gloplacha.2006.06.007.

Jin, Y.G., Wang, Y., Wang, W., Shang, Q.H., Cao, C.Q., and Erwin, D.H., 2000, Pattern of marine mass extinction near the Permian-Triassic boundary in South China: Science, v. 289, p. 432–436, doi:10.1126/science.289.5478.432.

Kearsey, T., Twitchett, R.J., Price, G.D., and Grimes, S.T., 2009, Isotope excursions and palaeotemperature estimates from the Permian/Triassic boundary in the southern Alps (Italy): Palaeogeography, Palaeoclimatology, Palaeoecology, v. 279, p. 29–40, doi:10.1016/j.palaeo.2009.04.015.

Kenig, F., Hudson, J.D., Sinninghe Damste, J.S., and Popp, B.N., 2004, Intermittent euxinia: Reconciliation of a Jurassic black shale with its biofacies: Geology, v. 32, p. 421–424, doi:10.1130/G20356.1.

Kennedy, M.J., Pevear, D.R., and Hill, R.J., 2002, Mineral surface control of organic carbon in black shale: Science, v. 295, p. 657–660, doi:10.1126/science.1066611.

Knoll, A.H., Summons, R.E., Waldbauer, J.R., and Zumberge, J., 2007, The geological succession of primary producers in the oceans, *in* Falkowski, P., and Knoll, A.H., eds., The Evolution of Primary Producers in the Sea: Boston, Academic Press, p. 133–163.

Korte, C., and Kozur, H.W., 2010, Carbon-isotope stratigraphy across the Permian-Triassic boundary: A review: Journal of Asian Earth Sciences, v. 39, p. 215–235, doi:10.1016/j.jseaes.2010.01.005.

Korte, C., Jasper, T., Kozur, H.W., and Veizer, J., 2005a, $\delta^{18}O$ and $\delta^{13}C$ of Permian brachiopods: A record of seawater evolution and continental glaciation: Palaeogeography, Palaeoclimatology, Palaeoecology, v. 224, p. 333–351, doi:10.1016/j.palaeo.2005.03.015.

Korte, C., Kozur, H.W., and Veizer, J., 2005b, $\delta^{13}C$ and $\delta^{18}O$ values of Triassic brachiopods and carbonate rocks as proxies for coeval seawater and palaeotemperature: Palaeogeography, Palaeoclimatology, Palaeoecology, v. 226, p. 287–306, doi:10.1016/j.palaeo.2005.05.018.

Korte, C., Pande, P., Kozur, H.W., Joachimski, M.M., and Oberhänsli, H., 2010, Massive volcanism at the Permian-Triassic boundary and its impact on the isotopic composition of the ocean and atmosphere: Journal of Asian Earth Sciences, v. 37, p. 293–311, doi:10.1016/j.jseaes.2009.08.012.

Kozur, H.W., 2004, Pelagic uppermost Permian and the Permian-Triassic boundary conodonts of Iran: Part I. Taxonomy: Hallesches Jahrbuch für Geowissenschaften, ser. B, Geologie, Palaontologie, Mineralogie, v. 18, p. 39–68.

Kozur, H.W., 2005, Pelagic uppermost Permian and Permian-Triassic boundary conodonts of Iran. Part II: Investigated sections and evaluation of the conodont faunas: Hallesches Jahrbuch für Geowissenschaften, ser. B, Geologie, Palaontologie, Mineralogie, v. 19, p. 49–86.

Kozur, H.W., and Weems, R.E., 2011, Detailed correlation and age of continental late Changhsingian and earliest Triassic beds: Implications for the role of the Siberian Trap in the Permian-Triassic biotic crisis: Palaeogeography, Palaeoclimatology, Palaeoecology, v. 308, p. 22–40, doi:10.1016/j.palaeo.2011.02.020.

Kuypers, M.M.M., van Breugel, Y., Schouten, S., Erba, E., and Sinninghe Damste, J.S., 2004, N_2-fixing cyanobacteria supplied nutrient N for Cretaceous oceanic anoxic events: Geology, v. 32, p. 853–856, doi:10.1130/G20458.1.

Lehrmann, D.J., Payne, J.L., Pei, D., Enos, P., Ellwood, B., Orchard, M.J., Zhang, J., and Wei, J., 2007, Record of the end Permian extinction and Triassic biotic recovery in the Chongzuo-Pingguo Platform, southern Nanpanjiang Basin, Guangxi, South China: Palaeogeography, Palaeoclimatology, Palaeoecology, v. 252, p. 200–217, doi:10.1016/j.palaeo.2006.11.044.

Leventhal, J.S., 1983, An interpretation of carbon and sulfur relationships in Black Sea sediments as indicators of environments of deposition: Geochimica et Cosmochimica Acta, v. 47, p. 133–137, doi:10.1016/0016-7037(83)90097-2.

Looy, C.V., Twitchett, R.J., Dilcher, D.L., van Konijnenburg-van Cittert, J.H.A., and Visscher, H., 2001, Life in the end-Permian dead zone: Proceedings of the National Academy of Sciences of the United States of America, v. 98, p. 7879–7883, doi:10.1073/pnas.131218098.

Luo, G., Wang, Y., Yang, H., Algeo, T.J., Kump, L.R., Huang, J., and Xie, S., 2011, Stepwise and large-magnitude negative shift in $\delta^{13}C_{carb}$ preceded the main marine mass extinction of the Permian-Triassic crisis interval: Palaeogeography, Palaeoclimatology, Palaeoecology, v. 299, p. 70–82, doi:10.1016/j.palaeo.2010.10.035.

Lyons, T.W., 1997, Sulfur isotopic trends and pathways of iron sulfide formation in upper Holocene sediments of the anoxic Black Sea: Geochimica et Cosmochimica Acta, v. 61, p. 3367–3382, doi:10.1016/S0016-7037(97)00174-9.

Lyons, T.W., and Berner, R.A., 1992, Carbon-sulfur-iron systematics of the uppermost deep-water sediments of the Black Sea: Chemical Geology, v. 99, p. 1–27, doi:10.1016/0009-2541(92)90028-4.

Lyons, T.W., and Severmann, S., 2006, A critical look at iron paleoredox proxies based on new insights from modern euxinic marine basins: Geochimica et Cosmochimica Acta, v. 70, p. 5698–5722, doi:10.1016/j.gca.2006.08.021.

Maynard, J.B., 1992, Chemistry of modern soils as a guide to interpreting Precambrian paleosols: The Journal of Geology, v. 100, p. 279–289, doi:10.1086/629632.

McCormick, M.P., Thomason, L.W., and Trepte, C.R., 1995, Atmospheric effects of the Mt. Pinatubo eruption: Nature, v. 373, p. 399–404, doi:10.1038/373399a0.

Mei, S., 1996, Restudy of conodonts from the Permian-Triassic boundary beds at Selong and Meishan and the natural Permian-Triassic boundary, *in* Wang, H., and Wang, X., eds., Memorial Volume of Prof. Sun Yunzhu: Palaeontology and Stratigraphy: Wuhan, China, China University of Geosciences Press, p. 141–148.

Mei, S., and Henderson, C.M., 2001, Evolution of Permian conodont provincialism and its significance in global correlation and paleoclimatic implication: Palaeogeography, Palaeoclimatology, Palaeoecology, v. 170, p. 237–260, doi:10.1016/S0031-0182(01)00258-9.

Mei, S., Zhang, K.X., and Wardlaw, B.R., 1998, A refined succession of Changhsingian and Griesbachian neogondolellid conodonts from the Meishan section, candidate of the global stratotype section and point of the Permian-Triassic boundary: Palaeogeography, Palaeoclimatology, Palaeoecology, v. 143, p. 213–226, doi:10.1016/S0031-0182(98)00112-6.

Mei, S., Henderson, C.M., and Jin, Y., 1999, Permian conodont provincialism, zonation and global correlation: Permophiles, v. 35, p. 9–16.

Meyer, K.M., Kump, L.R., and Ridgwell, A., 2008, Biogeochemical controls on photic-zone euxinia during the end-Permian mass extinction: Geology, v. 36, p. 747–750, doi:10.1130/G24618A.1.

Meyers, P.A., 1994, Preservation of elemental and isotopic source identification of sedimentary organic matter: Chemical Geology, v. 114, p. 289–302, doi:10.1016/0009-2541(94)90059-0.

Moldowan, J.M., Sundararaman, P., and Schoell, M., 1986, Sensitivity of biomarker properties to depositional environment and/or source input in the Lower Toarcian of S.W. Germany: Organic Geochemistry, v. 10, p. 915–926, doi:10.1016/S0146-6380(86)80029-8.

Mundil, R., Pálfy, J., Renne, P.R., and Brack, P., 2010, The Triassic timescale: New constraints and a review of geochronological data, *in* Lucas, S.G., ed., The Triassic Timescale: Geological Society of London Special Publication 334, p. 41–60.

Nassichuk, W.W., Thorsteinsson, R., and Tozer, E.T., 1973, Permian-Triassic boundary in the Canadian Arctic Archipelago, *in* Logan, A., and Hills, L.V., eds., The Permian and Triassic Systems and their Mutual Boundary: Canadian Society of Petroleum Geologists Memoir 2, p. 286–293.

Nesbitt, H.W., and Young, G.M., 1982, Early Proterozoic climates and plate motions inferred from major element chemistry of lutites: Nature, v. 299, p. 715–717, doi:10.1038/299715a0.

Nielsen, J.K., and Shen, Y., 2004, Evidence for sulfidic deep water during the Late Permian in the East Greenland Basin: Geology, v. 32, p. 1037–1040, doi:10.1130/G20987.1.

Obermajer, M., Stewart, K.R., and Dewing, K., 2007, Geological and Geochemical Data from the Canadian Arctic Islands: Part II. Rock Eval/TOC Data: Geological Survey of Canada Open-File 5459, CD-ROM.

Orchard, M.J., and Krystyn, L., 1998, Conodonts of the lowermost Triassic of Spiti, and new zonation based on *Neogondolella* successions: Rivista Italiana di Paleontologia e Stratigrafia, v. 104, no. 3, p. 341–368.

Orchard, M.J., Nassichuk, W.W., and Rue, L., 1994, Conodonts from the Lower Griesbachian *Otoceras latilobatum* bed of Selong, Tibet, and the position of the Permian-Triassic boundary, *in* Embry, A.F., Beauchamp, B., and Glass, D.J., eds., Pangea: Global Environments and Resources: Canadian Society of Petroleum Geologists Memoir 17: Calgary, Alberta, Canada, p. 823–843.

Ourisson, G., Albrecht, P., and Rohmer, M., 1979, The hopanoids: Palaeochemistry and biochemistry of a group of natural products: Pure and Applied Chemistry, v. 51, p. 709–729, doi:10.1351/pac197951040709.

Overmann, J., Cypionka, H., and Pfenning, N., 1992, An extremely lowlight-adapted phototrophic sulfur bacterium from the Black Sea: Limnology and Oceanography, v. 37, p. 150–155, doi:10.4319/lo.1992.37.1.0150.

Payne, J., and van de Schootbrugge, B., 2007, Life in Triassic oceans: Links between benthic and planktonic recovery and radiation, *in* Falkowski, P.G., and Knoll, A.H., eds., The Evolution of Primary Producers in the Sea: New York, Academic Press, p. 165–189.

Pearce, J.A., 1996, A user's guide to basalt discrimination diagrams, *in* Wyman, D.A., ed., Trace Element Geochemistry of Volcanic Rocks: Applications for Massive Sulphide Exploration: Winnipeg, Canada, Geological Association of Canada, p. 79–113.

Peters, K.E., Walters, C.C., and Moldowan, J.M., eds., 2004, The Biomarker Guide (2nd ed.): Cambridge, UK, Cambridge University Press, 490 p.

Plafker, G., and Berg, H.C., 1994, Overview of the geology and tectonic evolution of Alaska, *in* Plafker, G., and Berg, H.C., eds., The Geology of Alaska: Boulder, Colorado, Geological Society of America, The Geology of North America, v. G-1, p. 989–1021.

Price, J.R., and Velbel, M.A., 2003, Chemical weathering indices applied to weathering profiles developed on heterogeneous felsic metamorphic parent rocks: Chemical Geology, v. 202, p. 397–416, doi:10.1016/j.chemgeo.2002.11.001.

Raiswell, R., and Berner, R.A., 1986, Pyrite and organic matter in Phanerozoic normal marine shales: Geochimica et Cosmochimica Acta, v. 50, p. 1967–1976, doi:10.1016/0016-7037(86)90252-8.

Raiswell, R., Buckley, F., Berner, R.A., and Anderson, T.F., 1988, Degree of pyritization of iron as a paleoenvironmental indicator of bottom-water oxygenation: Journal of Sedimentary Petrology, v. 58, p. 812–819.

Rampino, M.R., and Adler, A.C., 1998, Evidence for abrupt latest Permian mass extinction of foraminifera: Results of tests for the Signor-Lipps effect: Geology, v. 26, p. 415–418, doi:10.1130/0091-7613(1998)026<0415:EFALPM>2.3.CO;2.

Reichow, M.K., and 15 others, 2009, The timing and extent of the eruption of the Siberian Traps large igneous province: Implications for the end-Permian environmental crisis: Earth and Planetary Science Letters, v. 277, p. 9–20, doi:10.1016/j.epsl.2008.09.030.

Reid, C.M., James, N.P., Beauchamp, B., and Kyser, T.K., 2007, Faunal turnover and changing oceanography: Late Palaeozoic warm-to-cool water carbonates, Sverdrup Basin, Canadian Arctic Archipelago: Palaeogeography, Palaeoclimatology, Palaeoecology, v. 249, p. 128–159, doi:10.1016/j.palaeo.2007.01.007.

Retallack, G.J., 1995, Permian-Triassic extinction on land: Science, v. 267, p. 77–80, doi:10.1126/science.267.5194.77.

Retallack, G.J., 1999, Postapocalyptic greenhouse paleoclimate revealed by earliest Triassic paleosols in the Sydney Basin, Australia: Geological Society of America Bulletin, v. 111, p. 52–70, doi:10.1130/0016-7606(1999)111<0052:PGPRBE>2.3.CO;2.

Retallack, G.J., 2005, Earliest Triassic claystone breccias and soil-erosion crisis: Journal of Sedimentary Research, v. 75, p. 679–695, doi:10.2110/jsr.2005.055.

Riccardi, A., Kump, L.R., Arthur, M.A., and D'Hondt, S., 2007, Carbon isotopic evidence for chemocline upward excursions during the end-Permian event: Palaeogeography, Palaeoclimatology, Palaeoecology, v. 248, p. 73–81, doi:10.1016/j.palaeo.2006.11.010.

Rigby, J.K., 1987, Phylum Porifera, *in* Boardman, R.S., Cheetham, A.H., and Rowell, A.J., eds., Fossil Invertebrates: Palo Alto, California, Blackwell Scientific, p. 116–139.

Robock, A., 2002, Pinatubo eruption: The climatic aftermath: Science, v. 295, p. 1242–1244, doi:10.1126/science.1069903.

Rohmer, M., Bouvier-Nave, P., and Ourisson, G., 1984, Distribution of hopanoid triterpenes in prokaryotes: Journal of General Microbiology, v. 130, p. 1137–1150.

Schouten, S., Rijpstra, W.I.C., Kok, M., Hopmans, E.C., Summons, R.E., Volkman, J.K., and Sinninghe Damsté, J.S., 2001, Molecular organic tracers of biogeochemical processes in a saline meromictic lake (Ace Lake): Geochimica et Cosmochimica Acta, v. 65, p. 1629–1640, doi:10.1016/S0016-7037(00)00627-X.

Self, S., Blake, S., Sharma, K., Widdowson, M., and Sephton, S., 2008, Sulfur and chlorine in Late Cretaceous Deccan magmas and eruptive gas release: Science, v. 319, p. 1654–1657, doi:10.1126/science.1152830.

Sephton, M.A., Looy, C.V., Brinkhuis, H., Wignall, P.B., de Leeuw, J.W., and Visscher, H., 2005, Catastrophic soil erosion during the end-Permian biotic crisis: Geology, v. 33, p. 941–944, doi:10.1130/G21784.1.

Sheldon, N.D., 2006, Abrupt chemical weathering increase across the Permian-Triassic boundary: Palaeogeography, Palaeoclimatology, Palaeoecology, v. 231, p. 315–321, doi:10.1016/j.palaeo.2005.09.001.

Shen, J., Algeo, T.J., Zhou, L., Feng, Q., Yu, J., and Ellwood, B.B., 2012, Volcanic perturbations of the marine environment in South China preceding the latest Permian extinction event and their biotic effects: Geobiology, v. 10, p. 82–103.

Shen, S., Cao, C., Henderson, C.M., Wang, X., Shi, G.R., Wang, Y., and Wang, W., 2006, End-Permian mass extinction pattern in the northern peri-Gondwanan region: Palaeoworld, v. 15, p. 3–30, doi:10.1016/j.palwor.2006.03.005.

Shen, S.Z., and Mei, S.L., 2010, Lopingian (Late Permian) high-resolution conodont biostratigraphy in Iran with comparison to South China zonation: Geological Journal, v. 45, p. 135–161, doi:10.1002/gj.1231.

Shen, S.Z., Henderson, C.M., Bowring, S.A., Cao, C.Q., Wang, Y., Wang, W., Zhang, H., Zhang, Y.C., and Mu, L., 2010, High-resolution Lopingian (Late Permian) timescale of South China: Geological Journal, v. 45, p. 122–134, doi:10.1002/gj.1232.

Shen, S.-Z., Crowley, J.L., Wang, Y., Bowring, S.A., Erwin, D.H., Sadler, P.M., Cao, C.Q., Rothman, D.H., Henderson, C.M., Ramezani, J., Zhang, H., Shen, Y., Wang, X.-D., Wang, W., Mu, L., Li, W.-Z., Tang, Y.-G., Liu, X.-L., Liu, L.-J., Zeng, Y., Jiang, Y.-F., and Jin, Y.-G., ;2011, Calibrating the end-Permian mass extinction: Science, v. 334, p. 1367–1372.

Summons, R.E., and Powell, T.G., 1987, Identification of aryl isoprenoids in source rocks and crude oils: Biological markers for the green sulphur bacteria: Geochimica et Cosmochimica Acta, v. 51, p. 557–566, doi:10.1016/0016-7037(87)90069-X.

Summons, R.E., Jahnke, L.L., Hope, J.M., and Logan, G.A., 1999, 2-methylhopanoids as biomarkers for cyanobacterial oxygenic photosynthesis: Nature, v. 400, p. 554–557, doi:10.1038/23005.

Sutton, S.J., and Maynard, J.B., 1993, Sediment- and basalt-hosted regoliths in the Huronian Supergroup: Role of parent lithology in middle Precambrian weathering profiles: Canadian Journal of Earth Sciences, v. 30, p. 60–76, doi:10.1139/e93-006.

Sweet, W.C., 1970, Uppermost Permian and Lower Triassic conodonts of the Salt Range and Trans-Indus Ranges, West Pakistan, *in* Kummel, B., and Teichert, C., eds., Stratigraphic Boundary Problems, Permian and Triassic of West Pakistan: University of Kansas Geology Department Special Publication 4, p. 207–275.

Symons, D.T.A., and McCausland, P.J.A., 2006, Paleomagnetism of the Fort Knox Stock, Alaska, and rotation of the Yukon-Tanana terrane after 92.5 Ma: Tectonophysics, v. 419, p. 13–26, doi:10.1016/j.tecto.2006.04.001.

Taylor, S.R., and McLennan, S.M., 1995, The geochemical evolution of the continental crust: Reviews of Geophysics, v. 33, p. 241–265, doi:10.1029/95RG00262.

Thordarson, T., and Self, S., 2003, Atmospheric and environmental effects of the 1783–1784 Laki eruption: A review and reassessment: Journal of Geophysical Research (Atmosphere), v. 108, p. JD002042.

Thorsteinsson, R., 1974, Carboniferous and Permian Stratigraphy of Axel Heiberg Island and Western Ellesmere Island, Canadian Arctic Archipelago: Geological Survey of Canada Bulletin 224, 115 p.

Tong, J.N., Zhang, S.X., Zuo, J.X., and Xiong, X.Q., 2007, Events during Early Triassic recovery from the end-Permian extinction: Global and Planetary Change, v. 55, p. 66–80, doi:10.1016/j.gloplacha.2006.06.015.

Umazano, A.M., Bellosi, E.S., Visconti, G., Jalfin, G.A., and Melchor, R.N., 2009, Sedimentary record of a Late Cretaceous volcanic arc in central Patagonia: Petrography, geochemistry and provenance of fluvial volcaniclastic deposits of the Bajo Barreal Formation, San Jorge Basin, Argentina: Cretaceous Research, v. 30, p. 749–766, doi:10.1016/j.cretres.2008.12.015.

Utting, J., Goodarzi, F., Dougherty, B.J., and Henderson, C.M.B., 1989, Thermal Maturity of Carboniferous and Permian Rocks of the Sverdrup Basin, Canadian Arctic Archipelago: Geological Survey of Canada Paper 89-19, 20 p.

Volkman, J., Barrett, S., Blackburn, S., Mansour, M., Sikes, E., and Gelin, F., 1998, Microalgal biomarkers: A review of recent research developments: Organic Geochemistry, v. 29, p. 1163–1179, doi:10.1016/S0146-6380(98)00062-X.

Wang, C.J., and Visscher, H., 2007, Abundance anomaly of alkyldibenzofurans and alkylphenols in the marine sediments across Permian-Triassic boundary as indicators for end-Permian global terrestrial and marine ecosystem collapse based on the Meishan section, China: Palaeogeography, Palaeoclimatology, Palaeoecology, v. 252, p. 291–303, doi:10.1016/j.palaeo.2006.11.048.

Wang, Z., 1996, Recovery of vegetation from the terminal Permian mass extinction in North China: Review of Palaeobotany and Palynology, v. 91, p. 121–142, doi:10.1016/0034-6667(95)00069-0.

Ward, P.L., 2009, Sulfur dioxide initiates global climate change in four ways: Thin Solid Films, v. 517, p. 3188–3203, doi:10.1016/j.tsf.2009.01.005.

Weissert, H., Joachimski, M., and Sarnthein, M., 2008, Chemostratigraphy: Newsletters on Stratigraphy, v. 42, p. 145–179, doi:10.1127/0078-0421/2008/0042-0145.

Wignall, P.B., 2001, Large igneous provinces and mass extinctions: Earth-Science Reviews, v. 53, p. 1–33, doi:10.1016/S0012-8252(00)00037-4.

Wignall, P.B., 2007, The end-Permian mass extinction—How bad did it get?: Geobiology, v. 5, p. 303–309, doi:10.1111/j.1472-4669.2007.00130.x.

Wilkin, R.T., and Arthur, M.A., 2001, Variations in pyrite texture, sulfur isotope composition, and iron systematics in the Black Sea: Evidence for late Pleistocene to Holocene excursions of the O_2-H_2S redox transition: Geochimica et Cosmochimica Acta, v. 65, p. 1399–1416, doi:10.1016/S0016-7037(01)00552-X.

Winchester, J.A., and Floyd, P.A., 1977, Geochemical discrimination of different magma series and their differentiation products using immobile elements: Chemical Geology, v. 20, p. 325–343, doi:10.1016/0009-2541(77)90057-2.

Winguth, A.M.E., and Maier-Reimer, E., 2005, Causes of marine productivity and oxygen changes associated with the Permian-Triassic boundary: A reevaluation with ocean general circulation models: Marine Geology, v. 217, p. 283–304, doi:10.1016/j.margeo.2005.02.011.

Xie, S., Pancost, R.D., Yin, H., Wang, H., and Evershed, R.P., 2005, Two episodes of microbial change coupled with Permo/Triassic faunal mass extinction: Nature, v. 434, p. 494–497, doi:10.1038/nature03396.

Xie, S., Pancost, R.D., Huang, J., Wignall, P.B., Yu, J., Tang, X., Chen, L., Huang, X., and Lai, X., 2007, Changes in the global carbon cycle occurred as two episodes during the Permian-Triassic crisis: Geology, v. 35, p. 1083–1086, doi:10.1130/G24224A.1.

Yin, H., Zhang, K., Wu, S., and Peng, Y., 1996, Global correlation and definition of the Permian-Triassic boundary, *in* Yin, H., ed., The Palaeozoic-Mesozoic Boundary Candidates of Global Stratotype Section and Point of the Permian-Triassic Boundary: Wuhan, China, China University of Geosciences Press, p. 3–28.

Yin, H., Zhang, K., Tong, J., Yang, Z., and Wu, S., 2001, The global stratotype section and point (GSSP) of the Permian-Triassic boundary: Episodes, v. 24, p. 102–114.

Yin, H.F., Feng, Q.L., Lai, X.L., Baud, A., and Tong, J.N., 2007, The protracted Permo-Triassic crisis and multi-episode extinction around the Permian-Triassic boundary: Global and Planetary Change, v. 55, p. 1–20, doi:10.1016/j.gloplacha.2006.06.005.

Zhang, K., Tong, J., Shi, G.R., Lai, X., Yu, J., He, W., Peng, Y., and Jin, Y., 2007, Early Triassic conodont-palynological biostratigraphy of the Meishan D section in Changxing, Zhejiang Province, South China: Palaeogeography, Palaeoclimatology, Palaeoecology, v. 252, p. 4–23, doi:10.1016/j.palaeo.2006.11.031.

Science Editor: Christian Koeberl
Associate Editor: Brian R. Pratt

Manuscript Received 4 March 2011
Revised Manuscript Received 30 September 2011
Manuscript Accepted 5 October 2011

Printed in the USA

Addendum

Evidence for a diachronous Late Permian marine crisis from the Canadian Arctic region

Thomas Algeo, Charles M. Henderson, Brooks Ellwood, Harry Rowe, Erika Elswick, Steven Bates, Timothy Lyons, James C. Hower, Christina Smith, Barry Maynard, Lindsay E. Hays, Roger E. Summons, James Fulton, and Katherine H. Freeman

(v. 124, no. 9/10, doi: 10.1130/B30505.1)

The samples from the West Blind Fiord section analyzed for geochemistry in this study were collected in 1999 by the Geological Survey of Canada, namely by Steve Grasby and Benoit Beauchamp, and are the property of the Government of Canada.